https://doi.org/10.5194/wes-2025-250
Preprint. Discussion started: 28 November 2025


eawe european academy of wind energy
Open Access WIND ENERGY SCIENCE DISCUSSIONS

# Estimating annual energy production of wake mixing control strategies including comparisons to wake steering

Gopal R. Yalla[1], Kenneth Brown[1], Lawrence Cheung[2], Dan Houck[1], Nathaniel deVelder[1], and Balaji Jayaraman[3]

[1]Sandia National Laboratories, Albuquerque, NM, USA
[2]Sandia National Laboratories, Livermore, CA, USA
[3]GE Vernova Advanced Research, Niskayuna, NY, USA

**Correspondence:** Gopal R. Yalla (gyalla@sandia.gov)

**Abstract.** This study presents an estimation of the annual energy production (AEP) associated with active wake mixing (AWM) control strategies in a wind farm. To achieved this, we first conduct a series of high-fidelity large eddy simulations (LES) of a wind farm for various turbine layouts and control parameters. These simulations extend previous findings from two-turbine studies to a larger array of wind turbines, demonstrating the effectiveness of AWM in enhancing power generation, particularly in geometrically aligned wind farms situated in stable atmospheric boundary layers. The results indicate that while the conventional pulse method leads to the best performance for second-row turbines, the helix method leads to greater improvements in power generation for third-row turbines. Second, a framework for estimating the AEP associated with AWM strategies is developed within the FLOw Redirection and Induction in Steady-state (FLORIS) toolkit, using a new empirical Gaussian wake model. The FLORIS parameters are calibrated to the LES data and an optimization routine is established for determining the optimal use of AWM in a wind farm for maximizing AEP. AEP estimates are provided using Weibull data from the New York Bight for multiple turbine layouts and blade pitching amplitudes. Third, the AEP gains from wake mixing are compared to those from wake steering using the yaw optimization routines in FLORIS. The power performance is similar for both control methods, generally leading to power gains of $1\%$ to $3\%$ for the wind conditions where active wake mixing or steering is used, which translates to AEP gains that are mostly less than $1\%$ for the wind farm and control parameters considered in this study.



## 1 Introduction

In large wind farms, the wake of a wind turbine presents complications for nearby turbines, depending on the atmospheric conditions, turbine characteristics, and turbine siting. A primary goal of wind farm flow control strategies is therefore to reduce the negative impacts of the wake momentum deficit by leveraging the turbine as a flow actuator though intelligent scheduling

https://doi.org/10.5194/wes-2025-250
Preprint. Discussion started: 28 November 2025


eawe european academy of wind energy
Open Access WIND ENERGY SCIENCE DISCUSSIONS

of either blade pitch, rotor speed, or nacelle yaw (Meyers et al., 2022). These strategies intentionally adjust the settings of upstream turbines away from their optimal setpoints for the collective benefit of the entire wind farm. A promising approach is to actuate the inherent fluid-dynamic instabilities in the wake flow that accelerate mixing and energy recovery from the surrounding ambient flow. Most work to-date has focused on instabilities surrounding the tip vortex (i.e., mutual inductance instability) (Sørensen, 2011; Sarmast et al., 2014; Lignarolo et al., 2015), hub vortex (Iungo et al., 2013), or bluff-body shear flow (Medici and Alfredsson, 2006; Okulov et al., 2014). Whereas actuation of tip or hub vortices has a primary effect on the near-wake region of the wind turbine (Marten et al., 2020; Brown et al., 2022), excitation of Strouhal-based, bluff-body shear flow instabilities is promising because the structures are large scale and may permit more control authority. In this paper, the primary focus is on active wake mixing (AWM) techniques that aim to excite these large-scale Strouhal-based structures in the wake through periodic oscillations in the blade pitch.

AWM has mostly been studied in the context of one or two turbines, with research primarily focusing on practical benefits in terms of power increases over baseline controls, as well as the fluid dynamics underlying these gains. The performance of AWM in these studies is promising, consistently demonstrating increases in power ranging from several percent to even tens of percent, depending on the forcing strategy, turbine layout, and atmospheric conditions (Frederik et al., 2020c, b; Yılmaz and Meyers, 2018; Taschner et al., 2023; Frederik et al., 2020a; van Vondelen et al., 2025). Additionally, the fluid dynamical studies of AWM have been useful for optimizing control parameters through a better understanding of wake physics and the influence of atmospheric boundary layer (ABL) conditions on different forcing strategies (Korb et al., 2023; Cheung et al., 2024b; Brown et al., 2025; Yalla et al., 2025); these studies have also contributed to the development of several reduced-order wake models (Gutknecht et al., 2023; Li and Yang, 2024; Cheung et al., 2024a). Some research has also examined AWM in wind farms, generally corroborating the benefits observed in two-turbine studies and even suggesting advantages for mid-farm actuation or farm-level control strategies (Munters and Meyers, 2018; Gutknecht et al., 2024).

While the results of these previous studies are insightful, there is still a critical need for additional high-fidelity data to accurately assess and understand the performance of AWM in a wind farm. Moreover, the practical implementation of AWM in the field will primarily depend on reliable estimates of the annual energy production (AEP) associated with wake mixing across a wide range of wind farm layouts and atmospheric conditions. The problem of wind farm optimization is challenging, often requiring millions of model evaluations to find solutions (Thomas et al., 2023). Therefore, low-fidelity, steady-state, engineering models are often desired, such as the FLOw Redirection and Induction in Steady-state (FLORIS) tool (NREL, 2025). FLORIS is a widely-used wind farm simulation software designed for wind farm layout and control optimization. It includes several steady-state engineering wake models for predicting the time-averaged three-dimensional flow field and turbine power of a wind farm, taking into account turbine control settings and atmospheric parameters that characterize the incoming wind. The proper implementation of AWM in a wind farm will therefore require integrating wake mixing control strategies with a tool like FLORIS, along with an optimization framework for guiding the use of AWM in a wind farm. Lastly, a direct comparison between wake mixing and wake steering control strategies is missing in the literature, leaving wind farm designers without a means to assess which control strategy is preferred for a given site.

https://doi.org/10.5194/wes-2025-250
Preprint. Discussion started: 28 November 2025


eawe european academy of wind energy
Open Access WIND ENERGY SCIENCE DISCUSSIONS

This study aims to address these needs. First, the performance of several AWM strategies in a wind farm is evaluated using large eddy simulation (LES) of turbines represented by an actuator line model (ALM). The LES encompass a range of control parameters and turbine layouts, providing a high-fidelity comparison of forcing strategies for a wind farm situated in a stable ABL. Second, a framework for estimating the AEP associated with wake mixing technologies is developed in FLORIS using a new empirical Gaussian wake model. Building on the work of Frederik et al. (2024), a model for AWM is added to FLORIS, and the LES data is used to calibrate the FLORIS model parameters. A validation between the high and low fidelity data is provided, and then an optimization procedure is developed to select the AWM control parameters that maximize AEP for a given wind farm configuration. The FLORIS model is demonstrated using Weibull data gathered in the NY Bight, and estimates of AEP for a range of blade pitch amplitudes are provided. Finally, a comparison to wake steering is made for a range of different maximum yaw offset angles using the calibrated empirical Gaussian model and the existing yaw-optimization tools in FLORIS.

The remainder of this paper is organized as follows: The simulation setup for the LES is discussed in Sec. 2.1-2.3 including the LES solver, the measured inflow data and ABL precursor generation, the wind farm and grid layout, and the turbine model and controller specifications. The LES results are then detailed in Sec. 2.5. In Sec. 3, the FLORIS model is presented as well as the relevant parameters, the calibration process, and the AWM optimization routine. Finally, the AEP results for both wake mixing and wake steering are discussed in Sec. 4, and conclusions are provided in Sec. 5.

## 2 Large Eddy Simulation

### 2.1 LES solver

The simulations in this work were performed with the U.S. Department of Energy (DOE) ExaWind solver AMR-Wind (Sprague et al., 2020; Sharma et al., 2024), a massively parallel, block-structured adaptive-mesh, incompressible flow solver for wind turbine and wind farm simulations. The AMR-Wind solver uses a second-order finite-volume method with second-order temporal integration, based on the approximate projection method of Almgren et al. (1998) and Sverdrup et al. (2018). For the solution of ABLs and wind-farm physics, AMR-Wind includes the following body force terms: turbine actuator forcing, Boussinesq buoyancy, Coriolis forcing, and a body force to maintain the precursor-derived inflow condition when applying the inflow/outflow boundary conditions. Calculations were performed on the Summit and Frontier cluster at the Oak Ridge Leadership Computing Facility (OLCF), requiring 86,000-90,000 GPU-hours on 1800-2000 GPU's per simulation. Total mesh sizes varied between $1.6 \times 10^9$ to $1.85 \times 10^9$ grid cells.

### 2.2 Inflow conditions

The inflow conditions for this study were based on 1.6 years of floating lidar measurements from the NY Bight (Mason, 2022). The roses for wind speed and turbulence intensity are provided in Fig. 1, along with histograms of wind speed, turbulence intensity, and wind direction at hub height. As described in Brown et al. (2025), wind conditions from this dataset were distilled

https://doi.org/10.5194/wes-2025-250
Preprint. Discussion started: 28 November 2025


eawe european academy of wind energy
Open Access WIND ENERGY SCIENCE DISCUSSIONS

into the 9 different conditions shown in Table 1. Precursors were then generated to represent the stable ABL conditions from the Med. WS/Low TI case, which occurs with relative frequency and corresponds to Region 2 behavior of the IEA 15 MW turbine where the nominal blade pitch remains constant. Specifically, a negative ground temperature rate and a non-zero surface roughness were introduced in the precursor simulations to closely match mean hub-height and rotor-averaged statistics of the Med. WS/Low TI case. The simulated precursor results in a hub-height wind speed of 9.0 m/s, TI of 3.1%, a rotor averaged shear of 0.16, and a rotor-averaged veer of 8.94°. The simulated values for the hub-height wind speed, TI, and rotor-averaged shear agree well with the targets from the measurements, although the larger veer magnitude measured at the NY Bight proved difficult to recreate in LES (Brown et al., 2025). Nonetheless, the veer magnitude achieved in the simulations (8.94° over the rotor disk) is still significant enough to study the impacts of veer on the performance of the AWM strategies (Frederik et al., 2025a).

Due to the computational expense of the LES, only one wind condition is simulated, and the parameter sweep is instead focused on varying control and wind farm layout parameters. In terms of calibrating the FLORIS model in Sec 3, we are therefore implicitly assuming that the relative power gains from AWM are not strongly sensitive to the wind condition below certain wind speeds and TI levels (to be described in Sec. 3.3) and thus can be tuned to just one wind condition for computational expediency. The selection of this wind condition was made as follows. Using the data in Table 1 for the frequency of occurrence of different wind conditions in the Weibull distribution and Table 2 for the estimated power gains of a two-turbine array, we can perform a coarse calculation of the effective power gain across wind conditions for the special case of the wind direction fully aligned with the turbine columns. This value, $\Delta P$, is calculated using the weighted average

$$\Delta P = \frac{\sum_{i=1}^{n} \Delta P_{wind,i} n_{bins,i}}{\sum_{i=1}^{n} n_{bins,i}}, \tag{1}$$

where $\Delta P_{wind,i}$ are the percentages from cells of Table 2, $n_{bins,i}$ are the bin numbers from the corresponding cells of Table 1, and the summations are over the conditions with non-zero entries in Table 2. The calculated value of $\Delta P$, 6.44%, is most similar to $\Delta P$ from the Med. WS/Low TI conditions (i.e., 7.34%), providing justification for using this wind condition for tuning of the AWM-specific wake behavior and power gains in FLORIS.

### 2.3 Simulation Domain and Wind Farm Layout

The LES domain and wind farm layouts are shown in Fig. 2. The wind farms consist of nine IEA 15 MW turbines arranged in a $3 \times 3$ array situated inside a domain of size $10 \times 10 \times 10$ km. This wind farm layout is motivated by the recent work of Kasper (2025), who showed that a $3 \times 3$ array of wind turbines may be sufficient for representing larger wind farm effects including the dominant momentum recovery mechanisms. A background mesh with a resolution of 5 m is used throughout the domain, which is refined to 2.5 m resolution in the vicinity of the wind farm. There is a slight variation in the size of the refinement zone dependent on the orientation of the wind farm. In all of the LES cases, the inflow wind direction is fixed at 225°, and three orientation angles of the wind farm are considered: 225°, 180°, and 206.5° (see Fig. 2). The orientation angles of 225° and 180° feature direct geometric alignment of the turbine rows or turbine diagonals with the wind direction. These layouts are the primary focus of the LES study as they lead to waked environments for downstream turbines, which is where

https://doi.org/10.5194/wes-2025-250
Preprint. Discussion started: 28 November 2025


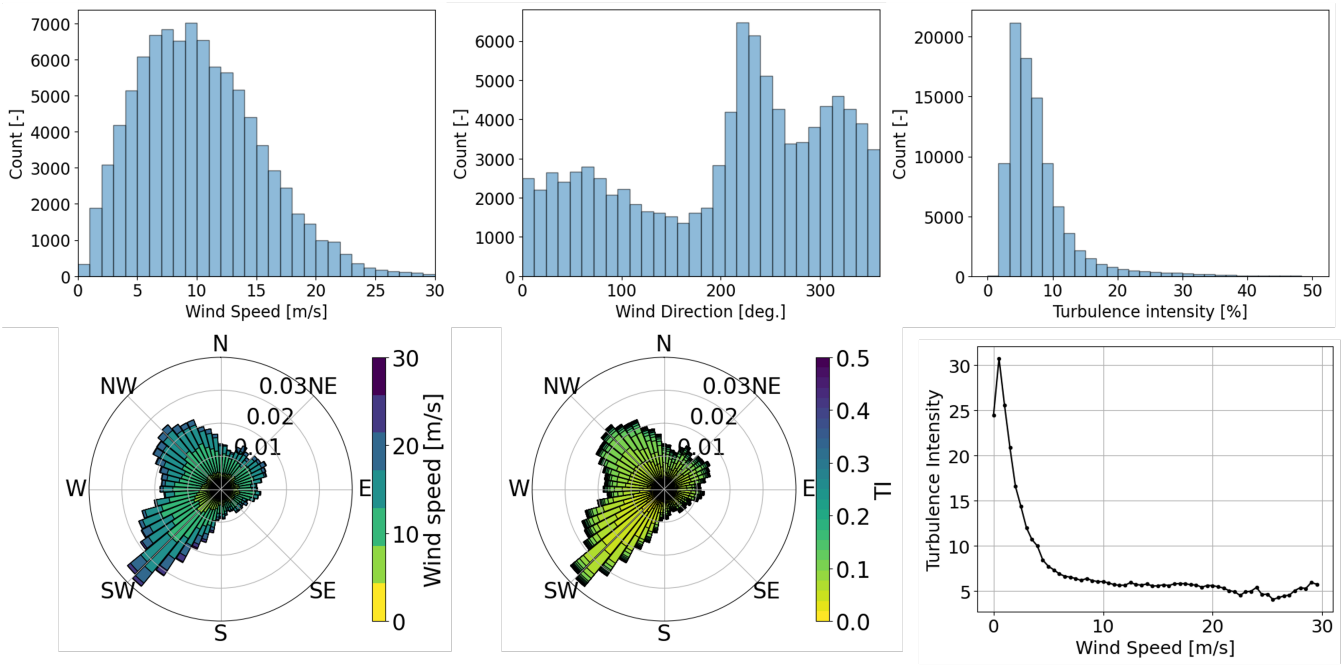


**Figure 1.** (Top) Histograms of wind speed, turbulence intensity, and wind direction at Site E06 in the NY Bight. (Bottom) Roses for wind speed and turbulence intensity, as well as turbulence intensity as a function of wind speed.

**Table 1.** Table recreated from Brown et al. (2025) describing the frequency of occurrence for different wind conditions from the measured data in the NY Bight. The percentage values refer to the percent of data within each wind-speed range for a given TI level, and the values in parenthesis are the corresponding number of 10-minute bins. The combined sum over a row does not add to 100% because of the filtering of some cases with poor power-law fits. The condition in bold is the one considered in the LES in this article.

| | Low TI ($\leq$5%) | Med. TI (5-10%) | High TI ($\geq$10%) | Combined TI |
|---|---|---|---|---|
| Low WS (6-7 m s$^{-1}$) | 24.3% (1856 bins) | 35.1% (2676 bins) | 18.5% (1414 bins) | 77.9% (5946 bins) |
| Med. WS (8.5-9.5 m s$^{-1}$) | **30.5% (2325 bins)** | 43.3% (3298 bins) | 13.0% (989 bins) | 86.8% (6612 bins) |
| High WS (11-12 m s$^{-1}$) | 30.3% (1910 bins) | 53.5% (3371 bins) | 9.7% (614 bins) | 93.5% (5895 bins) |

wake control is particularly beneficial. In contrast, the $206.5°$ case is included as a reference case where no downstream wake impingement occurs and the use of wake control is detrimental. This case is primarily included for calibration of the FLORIS model presented in Sec. 3. We refer to the turbine spacing of each wind farm as the shortest distance between two turbines in the farm. For the $3 \times 3$ turbine arrays orientated at $225°$, the turbine spacing therefore refers to the distance between successive turbine rows and columns. Turbine spacings of $5D$ and $6D$ are considered in the LES, which correspond to tightly spaced

https://doi.org/10.5194/wes-2025-250
Preprint. Discussion started: 28 November 2025


eawe european academy of wind energy
Open Access WIND ENERGY SCIENCE DISCUSSIONS

**Table 2.** Table derived from data in Frederik et al. (2025b) describing the power gains for two-turbine arrays in fully aligned wind conditions using the same computational setup as this article. Cells with non-zero data indicate the wind conditions where AWM will be taken to be enabled in our AEP estimation.

| | Low TI ($\leq$5%) | Med. TI (5-10%) | High TI ($\geq$10%) |
|---|---|---|---|
| Low WS (6-7 m s$^{-1}$) | 8.27% | 5.43% (estimated) | 0% (estimated) |
| Med. WS (8.5-9.5 m s$^{-1}$) | 7.34% | 5.43% | 0% (estimated) |
| High WS (11-12 m s$^{-1}$) | 8.49% | 5.43% (estimated) | 0% (estimated) |

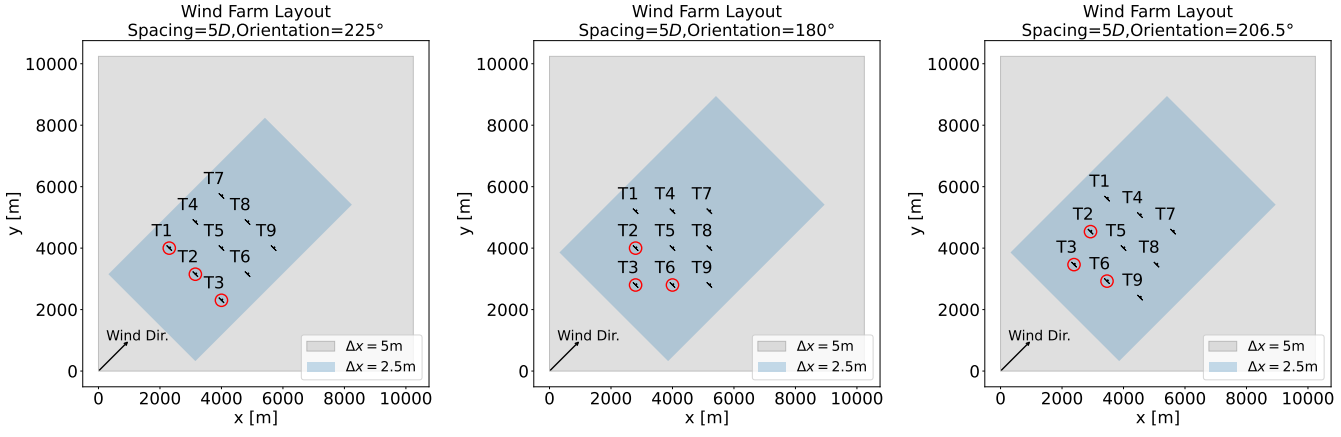


**Figure 2.** Horizontal planes from the LES domains. The 5 m background mesh and 2.5 m refinement region are indicated by the gray and blue rectangular regions, respectively. The panels show the $3 \times 3$ wind farm oriented at 225°, 180°, and 206.5°. For each layout, the nine turbines are labeled $T1 - 9$, and the turbines which are using AWM are circled in red. Specifically, $T1, T2, T3$ are actuated for the wind farm oriented at 225°, and $T2, T3, T6$ are actuated for the wind farms oriented at 180° and 206.5°.

wind farms that are well-suited for wake control, particularly in stable ABLs where wakes can persist tens of turbine diameters downstream. For each wind farm orientation angle, AWM is applied to three front-line turbines, as described in Fig. 2.

### 2.4 Turbine and Controller Specifications

The wind turbine model used in this study is the open-source IEA 15 MW (Gaertner et al., 2020). This turbine has a rotor diameter of $D = 240$ m, hub-height of 150 m, and rated power of 15 MW. The power and thrust curves, and additional design parameters, are included in Fig. 3. The turbine aerodynamic forces are computed using the OpenFAST software suite (National Renewable Energy Laboratory, 2024b), which has been validated at the megawatt scale for standalone simulations (Brown et al., 2024) and with coupling to LES (Hsieh et al., 2024), and which is coupled to AMR-Wind using an actuator line

https://doi.org/10.5194/wes-2025-250
Preprint. Discussion started: 28 November 2025


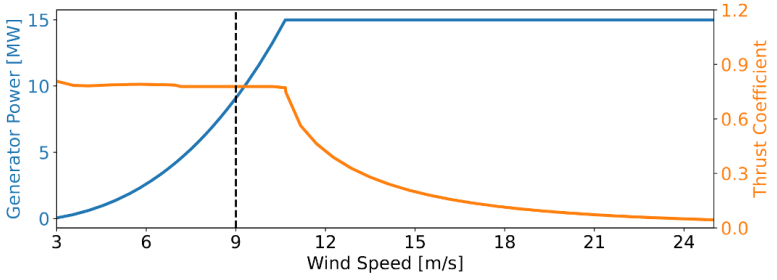


| IEA 15 MW | |
|---|---|
| Hub-height (m) | 150 |
| Rotor diameter (m) | 240 |
| Rated wind speed (m/s) | 10.59 |
| Design Ct | 0.804 |
| Rated TSR | 9.0 |

**Figure 3.** Specifications of the IEA 15 MW reference turbine model (Gaertner et al., 2020), including the generator power and rotor thrust curves (left) and the design parameters (right). The dashed line corresponds to the hub height wind speed for the Med. WS/Low TI precursor ABL simulation used in the LES.

model (ALM) (Sorensen and Shen, 2002). The ALM is defined with an isotropic Gaussian projection function with spreading parameter $\varepsilon/\Delta x = 0.8$, which was determined based on agreement with the OpenFAST power curve (uncoupled to an LES solver) in uniform wind conditions as described in Yalla (2024).

To implement the different control strategies on the IEA 15 MW turbine, NREL's reference open-source controller (ROSCO v2.8.0; National Renewable Energy Laboratory (2024a)) is used. AWM functionality was added to ROSCO v2.8.0 including both a normal-mode and Coleman-transform method. In this article, we choose to describe the normal-mode representation of AWM rather than the Coleman-transform representation, although both methods produce equivalent results as demonstrated in Cheung et al. (2024b). Following the derivation in Cheung et al. (2024b), the time series of pitch amplitude for a blade, $\theta_b(t)$ is

$$\theta_b(t) = \theta_0 + A\cos\left(\omega_e t - n\psi_b(t)\right). \tag{2}$$

where $\theta_0$ is the nominal blade-pitch command, $A$ is the pitch amplitude of each mode to be forced, $n$ is an azimuthal wavenumber, $\psi_b$ is the time series of blade azimuthal angle, and $\omega_e$ is an angular frequency, which can be specified through a Strouhal number, $St = \omega_e D/2\pi U_\infty$, where $U_\infty$ is the hub-height wind speed. While this implementation of AWM alters the blade-pitch control, it does not alter the baseline generator-torque control, which tracks optimum tip-speed ratio.

The azimuthal wavenumber, $n$, is typically used to distinguish between different AWM strategies. This paper primarily focuses on the case when $n = 0$, often referred to as the "pulse" method, in which an axisymmetric thrust variation is imparted on the wake through collective sinusoidal pitching of the three turbine blades. A single LES with $n = -1$ is also performed corresponding to the counter-clockwise "helix" method, which relies on individual pitch control to create a non-uniform thrust force around the rotor disk (Frederik et al., 2020b). The decision to focus on the pulse method is motivated by the work of Frederik et al. (2025a), who found that for a two-turbine array situated in a stable ABL with large veer, the pulse method outperforms other AWM strategies in terms of wake recovery rates, which Brown et al. (2025) primarily attributed to increased turbulent entrainment of mean streamwise velocity near the rotor's top-tip position.

https://doi.org/10.5194/wes-2025-250
Preprint. Discussion started: 28 November 2025


eawe european academy of wind energy
Open Access WIND ENERGY SCIENCE DISCUSSIONS

**Table 3.** Summary of LES cases.

| | AWC Parameters | | | Farm Layout | | Performance | |
|---|---|---|---|---|---|---|---|
| Forcing Strategy | Pitch Amplitude ($A$) | Strouhal Number (St) | Azimuthal Wavenumber ($n$) | Wind Farm Orientation | Turbine Spacing | Farm Power (MW) | Gain (%) |
| Baseline | 0° | N/A | N/A | 225° | $6D$ | 48.759 | N/A |
| Baseline | 0° | N/A | N/A | 225° | $5D$ | 44.959 | N/A |
| Baseline | 0° | N/A | N/A | 180° | $5D$ | 58.967 | N/A |
| Baseline | 0° | N/A | N/A | 206.5° | $5D$ | 76.692 | N/A |
| Pulse | 4° | 0.3 | 0 | 225° | $6D$ | 51.866 | 6.372 |
| Pulse | 4° | 0.3 | 0 | 225° | $5D$ | 48.192 | 7.191 |
| Pulse | 4° | 0.3 | 0 | 180° | $5D$ | 61.007 | 3.460 |
| $*$ Pulse | 4° | 0.3 | 0 | 206.5° | $5D$ | 75.425 | -1.652 |
| Pulse | 2° | 0.3 | 0 | 225° | $6D$ | 49.562 | 1.646 |
| CCW. Helix | 2° | 0.3 | -1 | 225° | $6D$ | 49.599 | 1.722 |
| Pulse | 4° | 0.15 | 0 | 225° | $6D$ | 50.051 | 2.649 |

$*$ This is a reference case where no downstream wake impingement occurs.

Similarly, a Strouhal number of $St = 0.3$ is primarily considered in this study, as previous studies across different AWM cases have shown strong control authority with this value (Frederik et al., 2020c; Munters and Meyers, 2018; Cheung et al., 2024b; Frederik et al., 2025a; Brown et al., 2025; Yalla et al., 2025). However, recent work by Li et al. (2024) suggests that forcing the wake at sub-harmonic frequencies may be advantageous in deep-array environments, because the flow structures are imparted on the wake over longer timescales. Therefore, a single LES of the pulse method forced at $St = 0.15$ is also performed to evaluate the effectiveness of sub-harmonic forcing strategies.

Lastly, the pitching amplitude, $A$, controls the strength of each forced azimuthal mode. The two values of $A$ used in the LES are $A = 2°$ and $4°$.

A full list of all the LES cases including the AWM control parameters and the wind farm layouts is provided in Table 3.

### 2.5 LES Results

The wind farm LES were allowed a transient run-out time of more than 13 minutes based on the time required for the wake of the frontline turbines to develop past the third row of turbines. Flow statistics were then accumulated at 2 Hz over 600 s, and averaged over a time interval of 6 complete Strouhal periods at $St = 0.3$, corresponding to $88.5$ s each. The statistics were computed over this integer number of Strouhal periods primarily to account for the large fluctuations in power introduced by the pulse actuation per Strouhal period (Frederik et al., 2020b).

https://doi.org/10.5194/wes-2025-250
Preprint. Discussion started: 28 November 2025


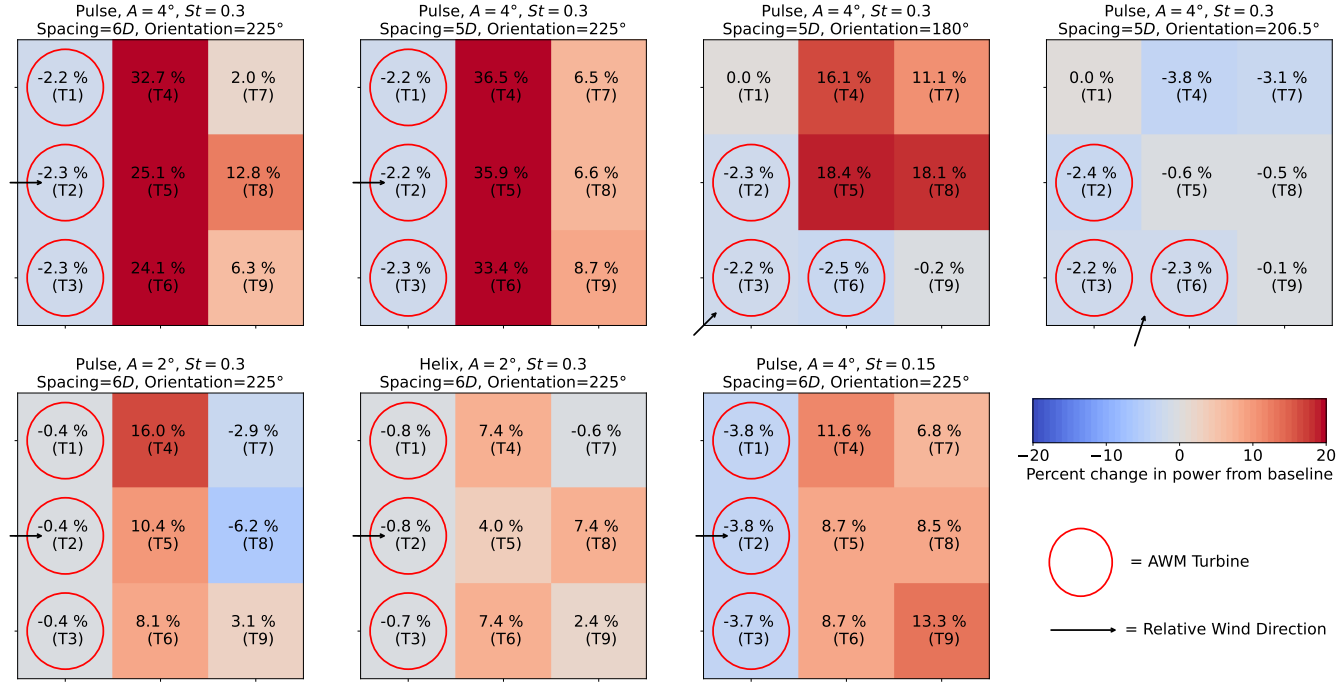


**Figure 4.** Performance of each turbine in the wind farms, relative to their respective baseline case. Each turbine is labeled $T1$-9 corresponding to the labels in Fig. 2. The actuated turbines are circled in red and the wind direction relative to the wind farm is indicated by the arrow.

The total time-averaged power generated by each wind farm is included in Table 3, along with the percent gain in power for each AWM strategy over the respective baseline case. There is a net gain in power for all AWM cases (except the reference case noted above) which ranges from a $1.65\%$ to a $7.19\%$ increase over the baseline depending on control parameters and turbine layout. As expected, for the same wind farm layout, the gain in power increases with pitch amplitude ($1.65\%$ at $A = 2°$ vs. $6.37\%$ at $A = 4°$) and inversely with turbine spacing ($6.37\%$ for $6D$ spacing vs. $7.19\%$ for $5D$ spacing). AWM is also more beneficial in fully-waked configurations ($7.19\%$ increase for the wind farm aligned with the wind direction at $225°$ vs. a $3.46\%$ increase for the wind farm oriented on the diagonal at $180°$). Interestingly, the helix case slightly outperforms the pulse method at the same pitching amplitude ($1.72\%$ vs. $1.65\%$), despite the strong performance of the pulse method over the helix method in the two-turbine array studies (Frederik et al., 2025a; Brown et al., 2025). In contrast, forcing at the subharmonic Strouhal number of $St = 0.15$ exhibits worse performance than the conventional Strouhal number $St = 0.3$ ($2.65\%$ vs. $6.37\%$).

The performance of each individual turbine in the wind farms is included in Fig. 4. The universal trend is that the actuated frontline turbines suffer power losses relative to the baseline, while the second and often third rows see an increase in power. Variability in the performance of each turbine row and column arises from fluctuations in the ABL over the 10-minute period, as well as potential farm-level blockage between exterior and interior rows. To better understand the average farm-level performance, the row-averaged power for the $6D$-spaced farms aligned with the wind direction is also shown in Fig. 5. On

https://doi.org/10.5194/wes-2025-250
Preprint. Discussion started: 28 November 2025


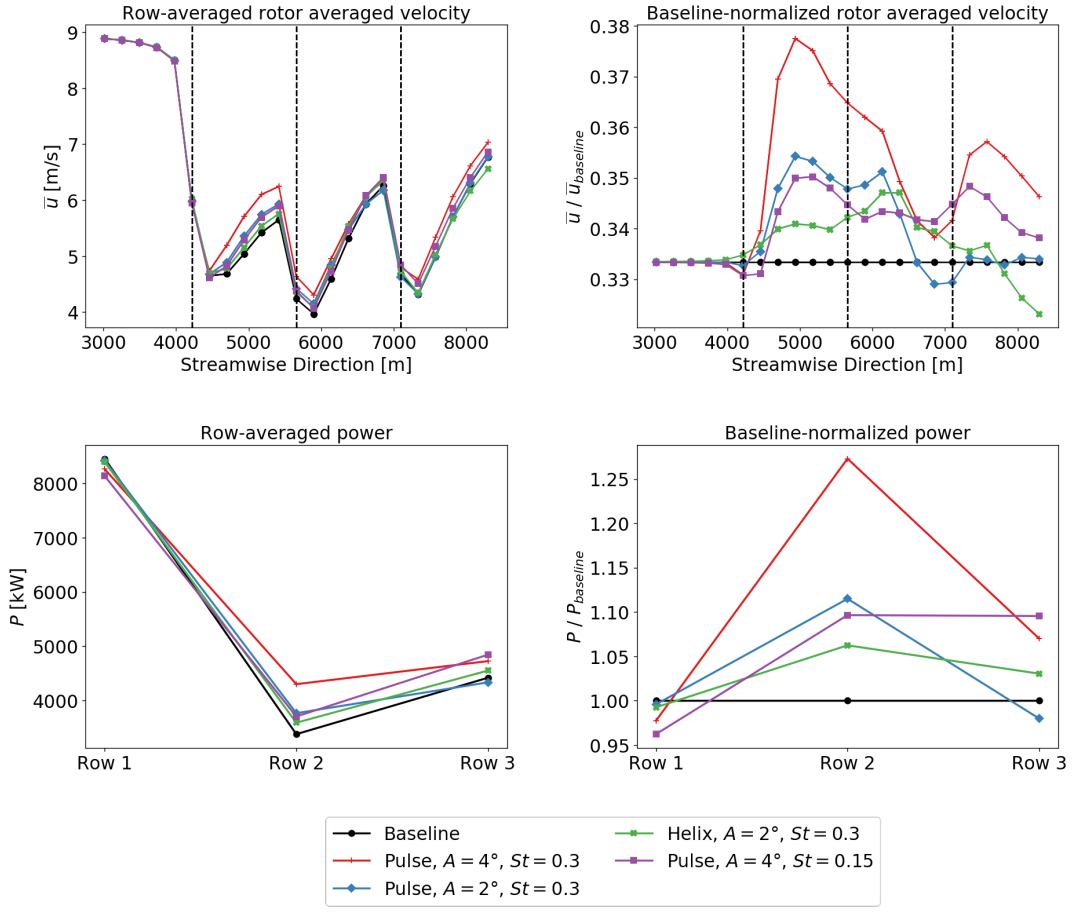


**Figure 5.** Row-averaged rotor-averaged velocity and power. Both the absolute and baseline-normalized values are shown. Included are results from the $6D$-spaced wind farms oriented with the wind direction at $225°$.

185 average, the second row turbines see increases in power that range from $5\%$ to $30\%$, with the pulse method forced at $St = 0.3$ outperforming both the helix method and the subharmonic forcing in the second row. However, the helix method maintains an increase in the third row of turbines, whereas the pulse method at the same pitch amplitude fails to exceed baseline values. Similarly, the subharmonic Strouhal forcing outperforms the conventional case in the third row turbines.

The baseline-normalized rotor-averaged velocities, also shown in Fig. 5, align with the trends observed in power, and also
190 suggest possible performance trends beyond the third row. In the wake of the third row of turbines, all pulse methods sustain an increase in rotor-averaged velocity compared to the baseline, whereas the helix case falls below the baseline levels. Notably, forcing at the conventional Strouhal number of $St = 0.3$ also leads to larger rotor-averaged velocities than the subharmonic forcing behind the third row.

https://doi.org/10.5194/wes-2025-250
Preprint. Discussion started: 28 November 2025


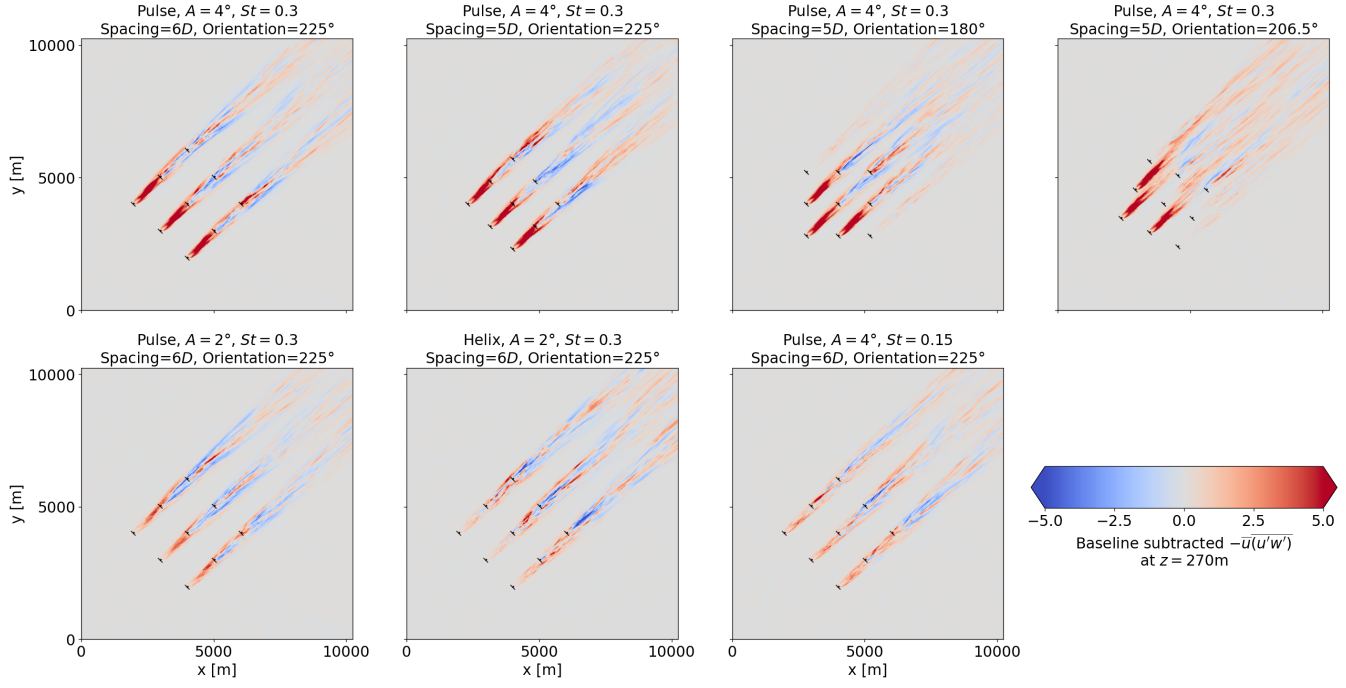


**Figure 6.** Baseline-subtracted contours of $-\overline{u}(\overline{u'w'})$ at $z = 270$ m, quantifying the turbulent entrainment of mean velocity into the wind farm.

Brown et al. (2025) linked the performance of AWM strategies primarily to the turbulent entrainment of mean velocity above the wind farm. This is the primary mechanism that re-energizes conventional wind farm between turbine rows, and this mechanism is enhanced by wake mixing. Entrainment of mean velocity into the farm is quantified here through the turbulent transport term $-\overline{u}\overline{u'w'}$, where $\overline{u}$ and $u'$ are the mean and fluctuating streamwise velocity, respectively, and $w'$ is the fluctuating vertical velocity. The baseline-subtracted turbulent entrainment fields are shown in Fig. 6 on a horizontal plane at the rotor top-tip position at $z = 270$ m. The pulse method forced at $St = 0.3$ primarily enhances turbulent entrainment in the immediate wake of the actuated turbines, with larger entrainment observed for larger pitch amplitudes. However, the helix method increases entrainment in the wake of both the first and second row turbines, explaining the power increases observed in third row of turbines. Similarly, the subharmonic forcing case does not increase entrainment as much as the conventional pulse in the wake of the actuated turbines, but it does lead to more turbine entrainment in the wake of the second row turbines. These trends align with the wake deficits shown at the hub-height plane in Fig. 7.

Lastly, a three-dimensional visualization of the flow is included in Fig. 8. Isocontours of the Q-criterion ($Q = 0.05$) are shown for an entire wind farm and for the wake profiles behind an actuated turbine. There is not much interaction between the turbine columns evident in the isosurfaces, which agrees with the hub-height wake contours shown in Fig. 7. The effects of the different forcing strategies on the wake structure are also somewhat visible in the isosurfaces. All pulse cases exhibit more wake breakup at this isosurface level compared to the baseline case, with the $A = 4°$ case having a more visibly coherent

https://doi.org/10.5194/wes-2025-250
Preprint. Discussion started: 28 November 2025


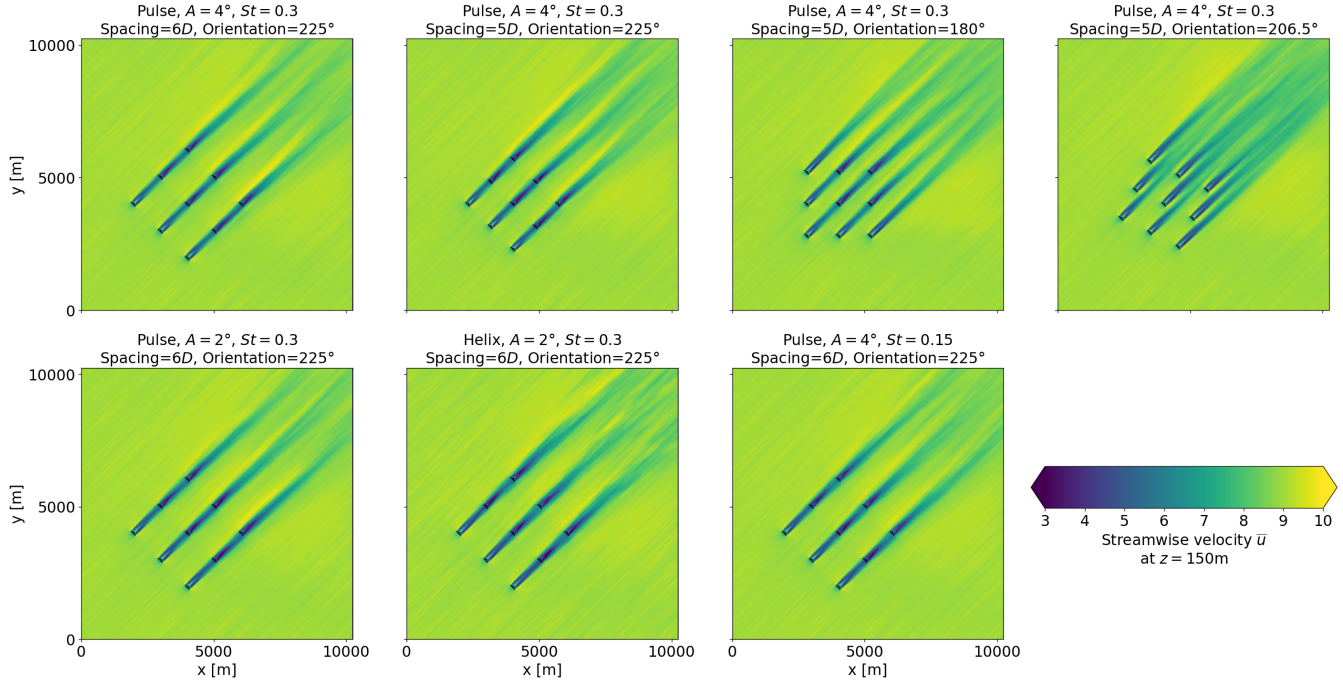


**Figure 7.** Streamwise velocity contours on the hub-height plane at $z = 150$ m.

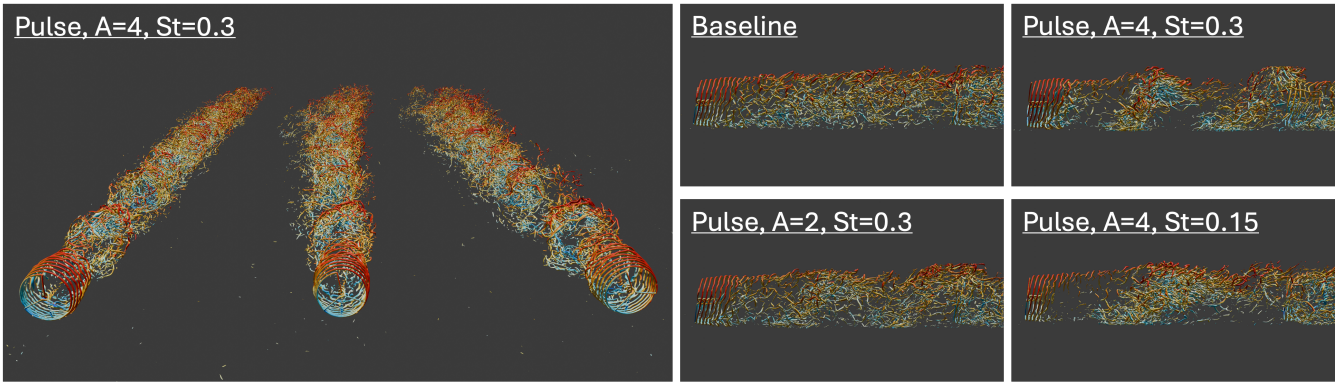


**Figure 8.** Flow visualization showing isosurfaces of the Q-criterion at $Q = 0.05$, colored by streamwise velocity. (Left) Isosurfaces of the $6D$-spaced wind farm, oriented with the wind direction at 225°, with pulse actuation at $A = 4°$ and $St = 0.3$. (Right) Wake profiles behind the actuated turbines for the baseline case and three different implementations of the pulse method.

https://doi.org/10.5194/wes-2025-250
Preprint. Discussion started: 28 November 2025


eawe european academy of wind energy
Open Access WIND ENERGY SCIENCE DISCUSSIONS

structure passing through the wake than the $A = 2°$ case. Similarly, the forced coherent structure for the subharmonic case is more elongated in the wake than that in the conventional $St = 0.3$ case, since the structure at $St = 0.15$ is generated over longer timescales.

## 3 FLORIS Modeling

In this section, the empirical Gaussian model is described as well as the parameter calibration and AWM optimization process. The focus is on the pulse method forced at $St = 0.3$, since this encompasses the majority of the LES training data.

### 3.1 Reduced-order flow model

The empirical Gaussian model in FLORIS is used to represent the steady-state wind farm wakes. This model is designed for tuning to an available data source as demonstrated using, for instance, LES as in Doekemeijer et al. (2020) and Hsieh et al. (2025). The normalized wake velocity deficit, $u/U_\infty$, at each streamwise location, $x$, and around lateral and vertical wake centers, $\delta_y$, and $\delta_z$, is expressed as

$$u/U_\infty(x) = 1 - C\exp\left(-\frac{(y-\delta_y(x))^2}{2\sigma_y(x)^2} - \frac{(z-\delta_z(x))^2}{2\sigma_z(x)^2}\right), \tag{3}$$

$$\sigma_{y,z}(x) = \int_0^x \sum_{i=0}^{n} k_i \mathbf{1}_{[b_i,b_{i+1}]}(x')dx' + M_j(x)dx' + \sigma_{y_0,z_0}, \tag{4}$$

$$M_j(x) = \omega_v \sqrt{\left[\sum_{\substack{i=1\\ i\neq j}}^{N_{turb}} \left(\frac{\Omega_{ij}a_i}{((x_j-x_i)/D_i)^2}\right)^2 + \left(\frac{A_j^p}{d}\right)^2 + (\gamma I)^2\right]}, \tag{5}$$

where $j$ ranges from 1 to the total number of turbines, $N_{turb}$. There are several relevant parameters in Eqs. 3-5 for this study, which are described herein. The model for the velocity deficit in Eq. 3 depends on a scaling factor, $C$, and wake widths $\sigma_y$ and $\sigma_z$, which are given by Eq. 4. The wake widths are specified by a constant initial wake width, $\sigma_{y_0,z_0}$, and a set of parameters, $k_i$, that control the wake expansion rate between break-point locations $b_i$ and $b_{i+1}$. The user-manual recommends default values for the initial wake widths, $\sigma_{y,z_0}$, and scaling factor, $C$, that should be satisfactory for most applications, and anticipates that no more than 3 expansion rates (along with 2 break points) should be needed to describe the wake expansion ($n = 2$ in Eq. 4). These guidelines are followed here. More details on the general implementation of the empirical Gaussian model in FLORIS can be found in the code documentation (NREL, 2025).

For each turbine, the wake widths also include a mixing term, $M$, which represents three factors associated with wake mixing that contribute to wake expansion (see Eq. 5). The first term in $M$ quantifies increased wake mixing due to overlapping wakes from multiple turbines. The matrix $\Omega_{ij}$ quantifies the area of overlap of the wake of turbine $i$ onto turbine $j$, and $a_i$ is the axial induction factor of the $i$th turbine. The second term in $M$ represents increased wake mixing due to AWM. Following Frederik et al. (2024), a power-law relationship is assumed, dependent on the blade-pitch amplitude, $A$. The exponent, $p$, and denominator, $d$, require tuning for different AWM strategies. In this work, the FLORIS model is calibrated for a fixed Strouhal

https://doi.org/10.5194/wes-2025-250
Preprint. Discussion started: 28 November 2025


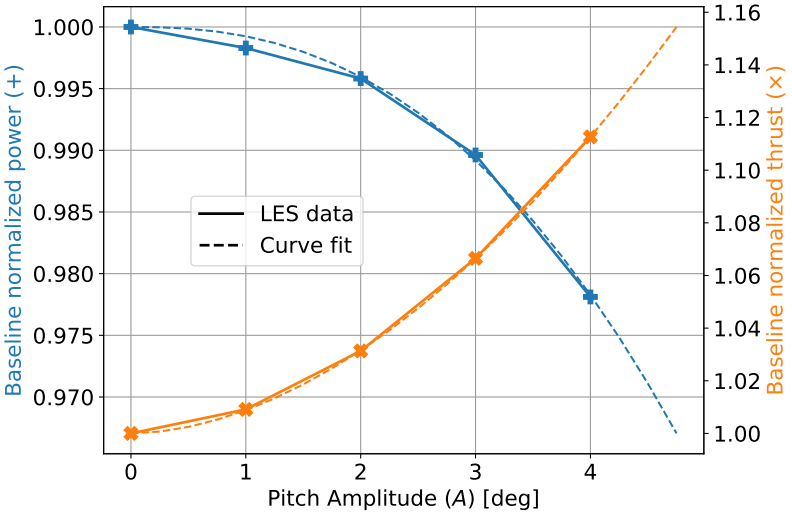


**Figure 9.** Assessment of the mean power and thrust of active turbines as a function of the AWM pitch amplitude, $A$. LES data is shown for five different values of $A$ ranging from $0°$ to $4°$. Additionally, a curve-fit of the data is shown of the form $1.0 + bA^a$ with values of $b = -7.54e\text{-}4$ and $a = 2.43$ for baseline-normalized power, and $b = 8.8e\text{-}3$ and $a = 1.84$ for baseline-normalized thrust.

number of $0.3$; however, in general, the wake expansion rate should also depend on Strouhal number. Lastly, the effects of atmospheric turbulence intensity on wake mixing are represented by the third term in $M$, in which the turbulence intensity level, $I$, is scaled by an adjustable parameter $\gamma$. These three terms are combined in a 2-norm to form $M$, and the strength of $M$ is controlled by the parameter $\omega_v$.

In addition to modeling wakes, the FLORIS model must also capture changes in the power and thrust of the turbines using AWM. To do so, a functional relationship between the AWM pitching amplitude and the power, $P_{\text{AWM}}$, and thrust coefficient, $C_{T_{\text{AWM}}}$, of the actuated turbines must be determined. Five LES were performed of a single actuated IEA 15 MW turbine using the pulse method with evenly spaced pitching amplitudes ranging from $A = 0°$ to $A = 4°$. The baseline-normalized generated power and thrust coefficient as a function of pitch amplitude are shown in Fig. 9. Also shown in Fig. 9 is a curve-fit of this data, which suggests that an appropriate model for the change in power and thrust of actuated turbines is of the form:

$$P_{\text{AWM}}/P_{\text{baseline}} = 1.0 + b_P A^{a_P} \tag{6}$$

$$C_{T_{\text{AWM}}}/C_{T_{\text{baseline}}} = 1.0 + b_{C_T} A^{a_{C_T}}. \tag{7}$$

These forms were implemented in the FLORIS model, with inputs for the four adjustable parameters, $b_P$, $a_p$, $b_{C_T}$, and $a_{C_T}$.

Lastly, due to discrepancies between the FLORIS database for power coefficient and LES, the power output of all turbines, whether using AWM or baseline controls, requires a small scaling factor (Doekemeijer et al., 2020). This is accomplished by scaling the wind speed in FLORIS by a wind speed factor, $W_{fact}$.

A list of all the parameters in the FLORIS model is provided in Table 4.

https://doi.org/10.5194/wes-2025-250
Preprint. Discussion started: 28 November 2025


eawe european academy of wind energy
Open Access WIND ENERGY SCIENCE DISCUSSIONS

### 3.2 Parameter tuning

**Table 4.** Fixed and calibrated FLORIS parameters used during the tuning process for this study.

| Parameter | Description | Value | Calibration step | Calibration range | Initial Guess |
|---|---|---|---|---|---|
| $\rho$ | Air Density | 1.2456 | 0 | Fixed | N/A |
| $\phi$ | Wind veer | 8.94 | 0 | Fixed | N/A |
| $\alpha$ | Wind shear | 0.16 | 0 | Fixed | N/A |
| $U$ | Wind Speed | 9.0 | 0 | Fixed | N/A |
| $\psi$ | Wind Direction | 225 | 0 | Fixed | N/A |
| $b_0$ | (1st) breakpoint | 0.0 | 0 | Fixed | N/A |
| $k_0$ | (1st) expansion rate | 3.64e-3 | 1 | (0.0,5.0) | 0.003 |
| $k_1$ | (2nd) expansion rate | 2.58e-2 | 1 | (0.0,5.0) | 0.02 |
| $k_2$ | (3rd) expansion rate | 6.85e-1 | 1 | (0.0,5.0) | 1.0 |
| $b_1$ | (2nd) breakpoint | 4.11 | 1 | (0.0,20.0) | 4.0 |
| $b_2$ | (3rd) breakpoint | 11.67 | 1 | (1.0,20.0) | 11.0 |
| $\gamma$ | Atmospheric TI gain | 0.1 | 1 | (0.0,0.1) | 0.05 |
| $\omega_v$ | Mixing gain velocity | 3.31 | 1 | (0,10.0) | 3.3 |
| $W_{\text{fact}}$ | Wind speed factor | 0.97 | 1 | (0,2.0) | 1.0 |
| $p$ | AWM exponent | 1.43 | 2 | (0.1,$\infty$) | 1.2 |
| $d$ | AWM denominator | 2029.86 | 2 | (100,$\infty$) | 400 |
| $b_P$ | AWM turbine power constant | -8.14e-4 | 2 | (-1e-3,-1e-5) | -7.54e-4 |
| $a_P$ | AWM turbine power exponent | 2.39 | 2 | (1.0,10.0) | 2.42 |
| $b_{C_T}$ | AWM turbine thrust constant | 1.88e-3 | 2 | (1e-4,0.01) | 8.84e-3 |
| $a_{C_T}$ | AWM turbine thrust exponent | 2.032 | 2 | (1.0,10.0) | 1.84 |

The FLORIS model parameters are calibrated to LES data using a two step process. First, the parameters not specific to AWM are tuned to the LES of the baseline wind farm cases. These parameters include the set of wake expansion rates ($k_i$), breakpoint locations ($b_i$), atmospheric TI gain ($\lambda$), wake mixing factor ($\omega_v$), and the wind speed factor ($W_{\text{fact}}$). Unlike the approach of Doekemeijer et al. (2020) that employs an objective function based on the difference in wake velocities between FLORIS and LES, we take an approach more inline with field calibrations where matching the power of turbines is the objective (Van Beek et al., 2021; van Binsbergen et al., 2024). Specifically, the baseline wake parameters are calibrated by minimizing the objective function,

$$J_{\text{step1}} = \sum_{j=0}^{N_{farms}} \sum_{i=0}^{N_{turb}} \left(P_{i,j}^{\text{FLORIS}} - P_{i,j}^{\text{LES}}\right)^2, \tag{8}$$

https://doi.org/10.5194/wes-2025-250
Preprint. Discussion started: 28 November 2025


eawe european academy of wind energy
Open Access WIND ENERGY SCIENCE DISCUSSIONS

where $P_{i,j}$ is the time-averaged generated power of the $i$th turbine in the $j$th wind farm case. In the second calibration step, the baseline wake parameters are held constant, and the AWM related parameters are calibrated to the actuated wind farm LES data. These parameters include the AWM exponent and denominator ($p$ and $d$), and the four parameters that model the power and thrust of the actuated turbines ($a_P$, $b_P$, $a_{C_T}$, $b_{C_T}$). The calibration of the AWM parameters is based on the change in power relative to the baseline case, rather than the absolute power values, i.e., the objective function is defined as follows

$$J_{\text{step2}} = \sum_{j=0}^{N_{\text{farms}}} \sum_{i=0}^{N_{\text{turbines}}} \left[ \left( P_{i,j}^{FLORIS,AWM} - P_{i,j}^{FLORIS,Baseline} \right) - \left( P_{i,j}^{LES,AWM} - P_{i,j}^{LES,Baseline} \right) \right]^2. \tag{9}$$

Table 4 includes the initial guess and range that was used to determine the parameters in each step of the calibration process. To facilitate each step of the calibration process, the optimization routines from scipy were used to minimize the cost functions for each set of calibration parameters. All of the LES cases presented in Sec. 2 were used for tuning the FLORIS parameters. This includes the four baseline LES cases, which were used in the first step of the calibration, and the five AWM LES cases, which were used in the second step of the calibration. The FLORIS parameters for air density, wind veer, wind shear, wind speed, and wind direction, were held constant in the FLORIS model to match the values from the LES precursor simulation (see Table 4).

A validation of the calibrated FLORIS model against the time-averaged LES training data is presented in Table 5. The relative error in total farm power ranges from magnitudes of 0.2% to 1.1% across the five AWM cases, corresponding to differences of 1 MW or less for the entire farm. Similarly, for all AWM cases, there is a good agreement in the total percent gain in power over the corresponding baseline cases between the FLORIS model and the LES data, with most cases agreeing to within half a percent.

Although the calibration above is performed with respect to farm power, a comparison of the calibrated FLORIS model with the time-averaged wake from an LES case is presented in Fig. 10 to provide insight on the residual errors in the FLORIS model. The most noticeable difference in the wakes on the hub-height plane is the omission of veer in the FLORIS model. Veer skews the LES wakes downstream, while the FLORIS wakes remain aligned with the incoming wind direction by design. This difference grows downstream, which is reflected in the difference of row-averaged power between the LES and FLORIS (also shown in Fig. 10). Similarly, profiles of the streamwise velocity in the wake of the turbines are compared in Fig. 11 for the LES and FLORIS model. Several modeling choices are evident in the FLORIS wake profiles, including the reduction of inflow wind speeds to account for induction effects, the symmetry of the wake profiles, uniformity of the wakes between turbine rows, and the reduced wake deficits to account for the absence of veer, which skews the wake profiles away from the downstream turbines in the LES, but only reduces the wake deficit in the FLORIS model and does not does alter the shape or skewness of the wakes.

### 3.3 AWM optimization process

To provide the maximal estimate of AEP, the optimal use of AWM is determined for each turbine within a given wind farm layout for every combination of wind speed, turbulence intensity, and wind direction in the Weibull data. A new python-based optimization routine was developed to evaluate all possible combinations of enabling or disabling AWM for each turbine,

https://doi.org/10.5194/wes-2025-250
Preprint. Discussion started: 28 November 2025


eawe european academy of wind energy
Open Access WIND ENERGY SCIENCE DISCUSSIONS

**Table 5.** Validation of the FLORIS model versus the LES training data

| Case Parameters | FLORIS Farm Power (MW) | LES Farm Power (MW) | FLORIS Gain (%) | LES Gain (%) |
|---|---|---|---|---|
| Pulse, $A = 4°$, $St = 0.3$ Spacing = $5D$, Angle = 225° | 48.434 | 48.192 | 7.309 | 7.191 |
| Pulse, $A = 4°$, $St = 0.3$ Spacing = $6D$, Angle = 225° | 51.538 | 51.866 | 5.314 | 6.372 |
| Pulse, $A = 4°$, $St = 0.3$ Spacing = $5D$, Angle = 180° | 61.361 | 61.007 | 3.626 | 3.460 |
| Pulse, $A = 2°$, $St = 0.3$ Spacing = $6D$, Angle = 225° | 50.125 | 49.562 | 2.428 | 1.646 |
| $*$ Pulse, $A = 4°$, $St = 0.3$ Spacing = $5D$, Angle = 206.5° | 75.206 | 75.425 | -1.138 | -1.652 |

$*$ The use of AWM is not recommended for this wind farm layout. It is included for model training purposes.

storing the setting that results in the highest total farm power for each wind condition. While a more computational efficient approach might use a geometric parameterization for wake-spreading to determine the likely waking or unwaking condition of downstream turbines (see Fig. A1 of Commission (2017)), the brute-force approach adopted herein is to simulate all possible combinations of active turbines, ensuring the best choice is determined. A single AEP estimate involves $\sim 90,000$ FLORIS evaluations, which took roughly 25 s to compute on a single core (using an Intel® Xeon® Platinum 8480+ processor). This time can be reduced by binning the Weibull data, although this is not done here to preserve the exact values of wind speed, wind direction, and turbulence intensity from the Weibull. Optimizing the use of AWM for a single wind farm layout using this approach took roughly 2 hours on a single node (112 cores) on the same machine.

In light of limited training data, several choices/assumptions are applied regarding AWM and the measured wind conditions to perform the optimization. The decision for two of the main assumptions, the ranges of WS and TI over which it is appropriate to apply the power gains from AWM, is aided by Table 2, where the non-zero entries indicate the wind conditions where the effect of AWM has been evaluated (or estimated) and found significant to justify use as follows. In agreement with intuition, the table suggests relatively constant percent power gains over the baseline with WS and diminishing gains with TI. Specifically, the effectiveness of AWM is expected to decrease at higher TI for a given streamwise spacing as increased ambient mixing reduces the benefit of externally-imposed mixing. As such, the highest TI category was not simulated and is conservatively assumed to produce no power benefit from AWM. With regards to WS, AWM is assumed to be useful throughout Region II and into early Region III according to Table 2. The utility of AWM is certain to diminish as WS increases higher in Region III due to the lower wake effects in this region, so an upper cutoff point of WS = 15 m/s is arbitrarily selected for this study. Thus,

https://doi.org/10.5194/wes-2025-250
Preprint. Discussion started: 28 November 2025


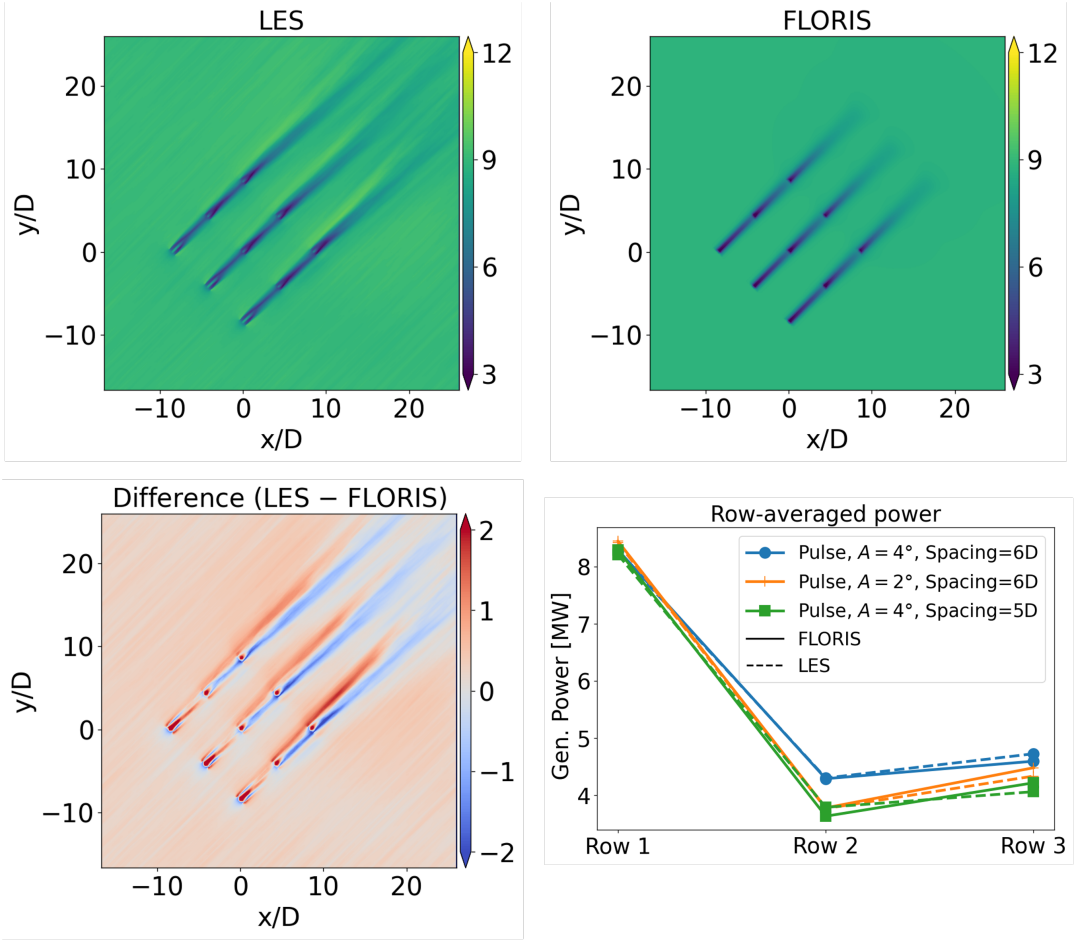


**Figure 10.** (Top) Hub-height plane of streamwise velocity contours (with units m/s) for the time-averaged LES field and the FLORIS model predictions. The pulse case with $A = 4°$ and $St = 0.3$ is shown for the $6D$-spaced wind farm layout oriented at 225°. (Bottom) The difference between the LES and FLORIS fields on the hub-height plane, and comparisons of row-averaged power for three LES and FLORIS cases.

the WS and TI ranges adopted for enabled AWM in this study are [cut-in, 15 m/s] and [0,10%], respectively. The optimization problem to maximize AEP for a given wind farm is stated formally below in Eqs. 10-13:

**Objective:**

$$\max_{\mathbf{x}} \; J_{AEP}(\mathbf{x}) = \sum_{\mathbf{w}\in\mathbf{W}} \sum_{i=0}^{N_{turbines}} P_i(x_i(\mathbf{w}), \mathbf{w}) \tag{10}$$

https://doi.org/10.5194/wes-2025-250
Preprint. Discussion started: 28 November 2025


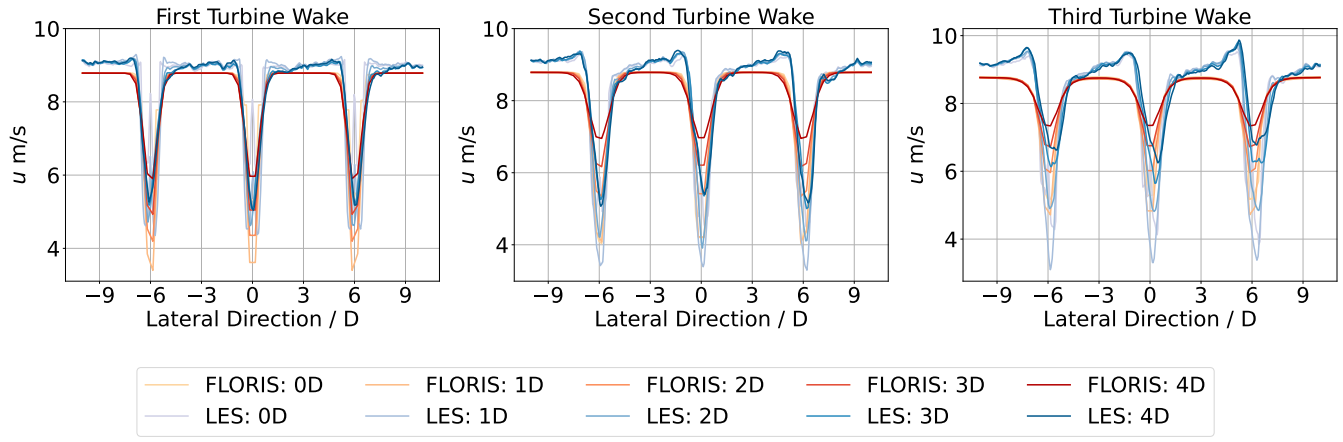


**Figure 11.** Hub-height profiles of the axial velocity in the wake of first, second, and third turbine rows. Shown are the LES and FLORIS results for the $6D$-spaced wind farm oriented at $225°$ with the pulse method at $A = 4°$ and $St = 0.3$.

**Subject to:**

$$\mathbf{x} = \mathbf{0} \text{ if } U > 15 \tag{11}$$

$$\mathbf{x} = \mathbf{0} \text{ if } I > 0.1 \tag{12}$$

$$\sum_{i=0}^{N_{turbine}} x_i \leq N_{\text{AWM}} \text{ (optional)} \tag{13}$$

where $P_i$ is the power of the $i$th turbine in the farm and $\mathbf{w} = [U, I, \psi]$ is a combination of wind speed, $U$, turbulence intensity level, $I$, and wind direction, $\psi$, from the set of all such combinations in the Weibull data, $\mathbf{W}$. For each wind condition, $\mathbf{w}$, the optimization parameter, $\mathbf{x}$, is an binary vector with a value of 1 if AWM is active for the $i$th turbine and 0 if not. Therefore, the total size of the optimization problem is governed by the cardinality of the Weibull set, $|\mathbf{W}|$, multiplied by the total number of possible uses of AWM throughout the farm for each wind condition, $2^{N_{turbine}}$. This is reduced by the constraints 11 and 12, which restrict the use of AWM above wind speeds of 15 m/s and TI levels above $10\%$, respectively. An additional constraint, 13, can be placed on the optimization problem to limit the number of actuated turbines in the farm by setting $N_{\text{AWM}} < N_{turbine}$. This feature can be used, for example, to restrict mid-farm actuation, ensuring that only three frontline turbines are actuated at any given time. However, no such restriction is applied here; all turbines are allowed to actuate if it benefits the total farm power, including downstream turbines, which has recently shown promise in the context of synchronize wake mixing strategies (van Vondelen et al., 2025). Note that the LES cases do not feature any configurations where AWM is applied to waked turbine, so this limitation of the training data should be borne in mind when interpreting results.

https://doi.org/10.5194/wes-2025-250
Preprint. Discussion started: 28 November 2025


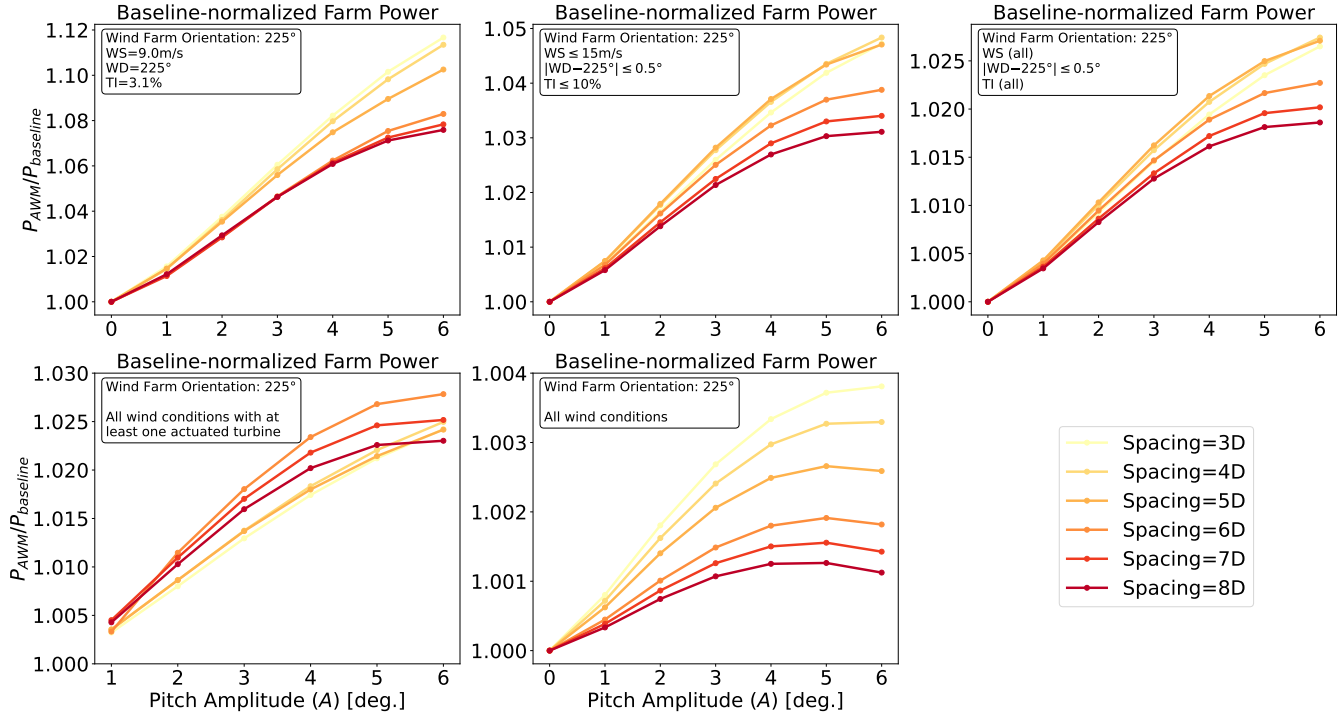


**Figure 12.** Baseline-normalized total farm power for the wake mixing cases as a function of the AWM pitch amplitude. The wind farm is oriented at 225° and the turbine spacing is varied from $3D$ to $8D$. In each panel, a different set of wind conditions from the Weibull distribution is considered, as indicated by the annotation in the top left corner of the panel.

## 4 AEP Results

### 4.1 Wake Mixing AEP Results

The primary utility of the FLORIS model in this work is to provide an estimate of AEP, which is a key economic indicator for wind farm flow control technologies. AEP gain is estimated for a $3 \times 3$ wind farm, similar to those in Sec. 2, but for a wider range of turbine layouts and AWM parameters. AEP is computed using the Weibull data gathered at Site E06 in the NY Bight. Histograms of wind directions, TI, and wind speed, as well as wind roses, at this site were shown previously in Fig. 1. In this section, AEP is examined as a function of two wind farm layout parameters including the wind farm orientation angle and the turbine spacing, as well as the AWM pitch amplitude.

In Fig. 12, the wind farm orientation angle is fixed at 225° and the FLORIS predictions of baseline-normalized farm power are shown for turbine spacings ranging from $3D$ to $8D$ and AWM pitch amplitudes ranging from $A = 1°$ to 6°. The results are shown for five different sets of wind conditions from the Weibull data including:

1. Wind Speed $= 9.0$ m/s, Wind Direction $= 225°$, TI $= 3.1\%$

https://doi.org/10.5194/wes-2025-250
Preprint. Discussion started: 28 November 2025


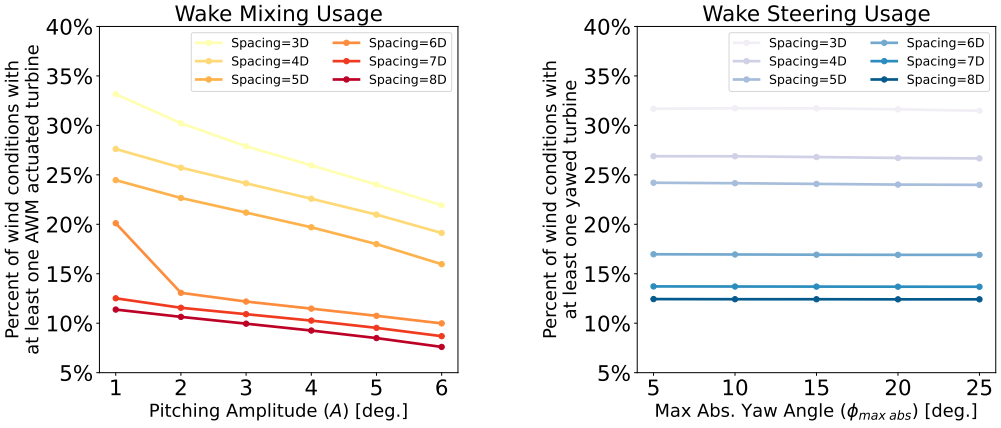


**Figure 13.** The usage of wake mixing (left) and wake steering (right) across all wind conditions in the Weibull distribution. For both control strategies, the wind farm is oriented at $225°$ and the turbine spacing is varied from $3D$ to $8D$. The percentages indicate the amount of wind conditions where the optimization routine actuated/yawed at least one turbine in the wind farm in order to maximize farm power.

2. Wind Speed $\leq 15.0$ m/s, Wind Direction $225° \pm 0.5°$, TI $\leq 10\%$
3. Wind Speed (all), Wind Direction $225° \pm 0.5°$, TI (all)
4. All wind speeds, wind directions, and TI where at least one turbine is using AWM to maximize farm power.
5. All wind speeds, wind directions, and TI in the Weibull.

These five sets of wind conditions are analyzed to illustrate the progression of power gains as the wind conditions vary from the type of ideal scenarios typically studied in wind farm flow control LES, to the comprehensive range of wind conditions that a turbine would typically encounter during annual operations. The first, second, third, and fifth sets of wind conditions are arranged from the least to the most comprehensive in terms of the total number of wind conditions considered from the Weibull data, with the power gains for each discussed below. The fourth set of wind conditions aims to contextualize these power gains by examining the frequency of AWM usage across all wind conditions in the Weibull distribution, which will be addressed in the following paragraph.

The first set of wind conditions correspond to an extrapolation of the LES data, and gains in power ranging from $1\%$ to $12\%$ are observed. These values are typical of those reported in AWM studies in low TI environments when the wind direction is directly aligned with the turbines (Frederik et al., 2020c, b; Yılmaz and Meyers, 2018; Taschner et al., 2023; Frederik et al., 2020a, 2025a; Yalla et al., 2025). In the second set of wind conditions, partial waking is allowed, while the wind speeds and TI levels are restricted to values where AWM is applicable. Gains in power over the baseline reduce to around $1\%$ to $5\%$, which are further reduced to $0.5\%$ to $2.5\%$ when all wind speeds and TI levels are considered for these partially-waked cases in the third set of wind conditions. In the fifth set of wind conditions shown in Fig. 12, the entire Weibull data is considered, providing

https://doi.org/10.5194/wes-2025-250
Preprint. Discussion started: 28 November 2025


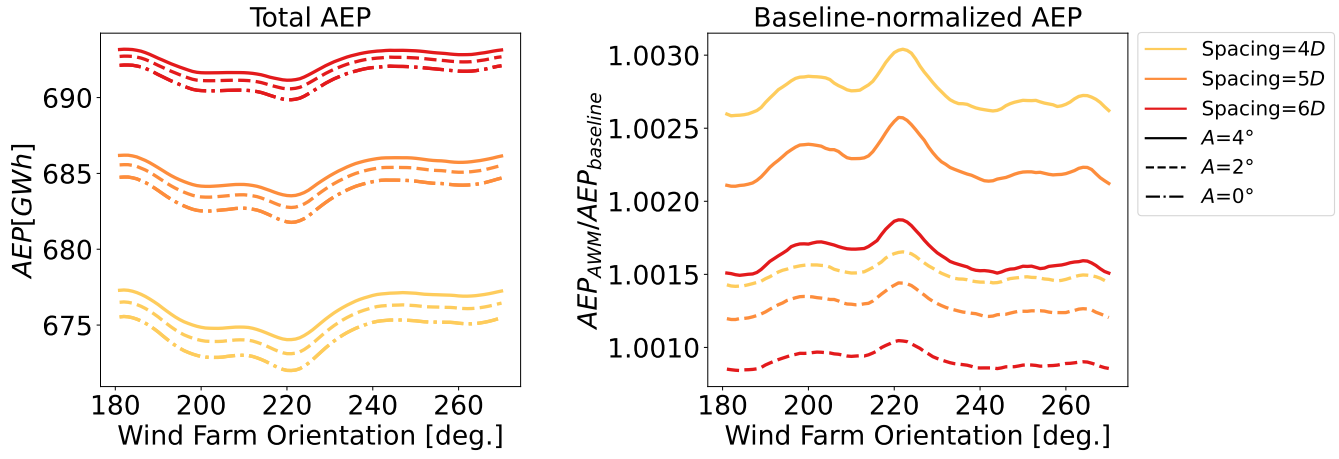


**Figure 14.** Absolute and baseline-normalized AEP as a function of the wind farm orientation angle at three different turbine spacings and two pitch amplitudes for the wake mixing cases.

an equivalent measure of AEP gains over baseline operations. In this case, the gains in AEP range from $0.1\%$ to $0.4\%$, which increase with increases in the AWM pitch amplitude and decreases in turbine spacings.

The fourth set of wind conditions shown in Fig. 12 only considers wind speeds, TI levels, and wind directions for which at least one turbine was actuated by the optimization routine to maximize the total wind farm power. The percent of wind conditions where AWM is used to maximize power is shown in Fig. 13. For smaller turbine spacings (3D-5D), AWM is used for $20\%$ to $35\%$ of the total number of wind conditions, with usage decreasing with pitch amplitude. For larger turbine spacings (6D-8D), AWM is used between roughly $10\%$ and $15\%$ of the time. For the wind conditions where AWM is used, the total farm power is increased by $1\%$ to $3\%$ over baseline operations (Fig. 12). Interestingly, these gains in power do not strictly decrease with turbine spacing, and the largest gains when using AWM are observed for a turbine spacing of 6D. In this sense, AWM is used more selectively for larger turbine spacings ($\geq$ 6D) than for smaller spacings ($\leq 5D$), leading to larger total gains in power when AWM is used.

The results discussed so far consider a wind farm orientation angle of $225°$, aligning with the predominant southwesterly and northwesterly directions in the wind rose. This corresponds to a turbine layout that is a worst-case scenario in terms of the waking of downstream turbines, and therefore a best-case scenario for wake mitigation control strategies. Although such layouts do exist (Shid-Moosavi et al., 2024), it is also important to consider the changes in AEP as a function of wind farm orientation angle. Fig. 14 shows the total AEP and baseline-normalized AEP as the angle of the wind farm is rotated $90°$ at $1°$ increments. Three different turbine spacings are considered ranging from $4D$ to $6D$, with two different pitch amplitudes, $A = 2°$ and $4°$, in addition to the baseline case. Total AEP increases with the turbine spacing and pitch amplitude, reaching a value of $> 690$ GWh for the $6D$ spaced farm with $A = 4°$. As expected, the largest benefit from AWM occurs for a wind farm angle of $225°$ for all turbine spacings and pitch amplitudes. As the wind farm is rotated away from the $225°$ orientation, the gains in AEP reduce by roughly $0.05\%$.

https://doi.org/10.5194/wes-2025-250
Preprint. Discussion started: 28 November 2025


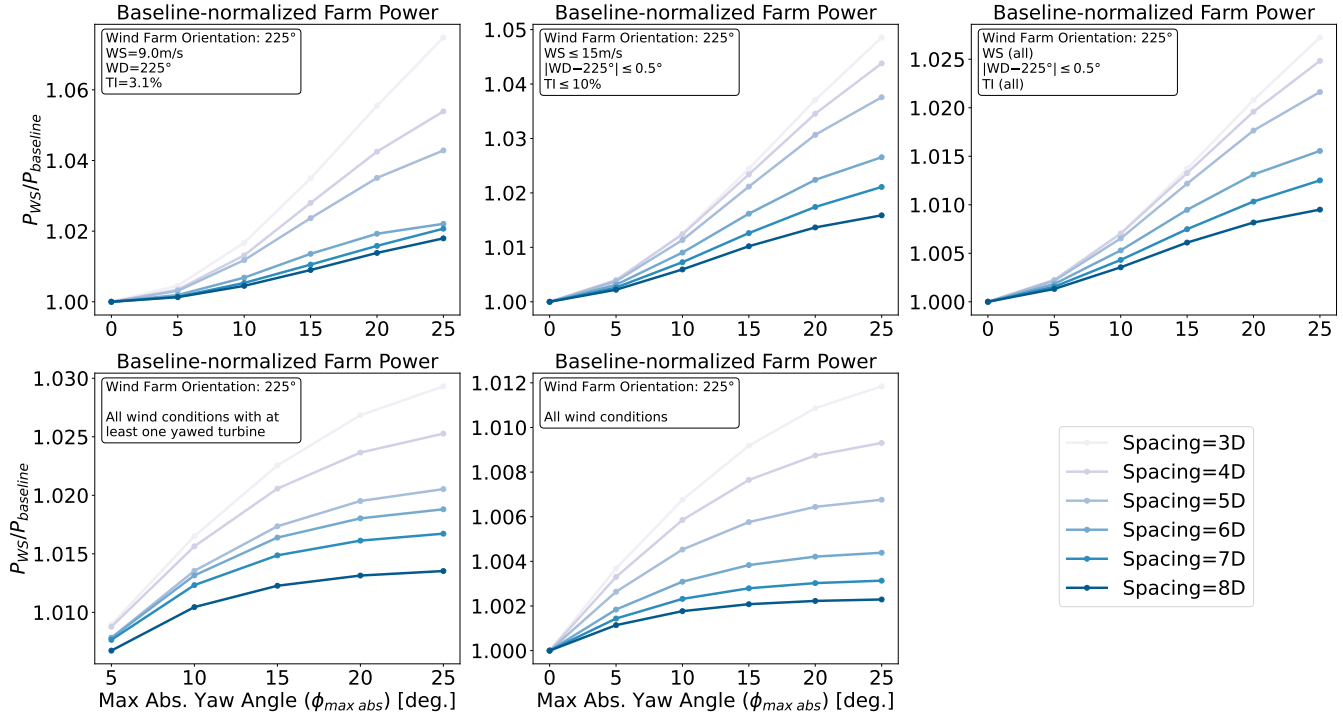


**Figure 15.** Baseline-normalized total farm power for the wake steering cases as a function of the maximum yaw offset angle. The wind farm is oriented at 225° and the turbine spacing is varied from $3D$ to $8D$. In each panel, a different set of wind conditions from the Weibull distribution is considered, as indicated by the annotation in the top left corner of the panel.

### 4.2 Wake Steering Results

Up to this point, the discussion has primarily centered on wake mixing and its implications for turbine performance and AEP. However, by using the empirical Gaussian model that was calibrated for the baseline wake in Sec. 3.2, we can leverage the built-in tools in FLORIS for wake steering to compare power gains between wake mixing and wake steering strategies. Specifically, the Serial-Refine method for quickly finding the optimal yaw angles in FLORIS is used to maximize farm power (Fleming et al., 2022). This method is taken to be the wake steering equivalent of the wake mixing optimizer developed in Sec. 3.3. As an analog to varying the blade pitch amplitude for wake mixing, the maximum absolute yaw angle, $\phi_{max\ abs}$, is varied from $\phi_{max\ abs} = 0°$ to 25° at 5° increments. For each value of $\phi_{max\ abs}$, the optimal yaw-offsets for each turbine are determined between $\pm\phi_{max\ abs}$ for all wind conditions in the Weibull distribution using the Serial-Refine method with a resolution of 1°. It is important to note that, unlike the AWM results where a fixed pitch amplitude is applied to actuated turbines, the Serial-Refine method selects the optimal value for each turbine between $\pm\phi_{max\ abs}$. For example, if $\phi_{max\ abs} = 25°$, turbines may still only be yawed 5° if optimal. Therefore, unlike wake mixing where actuation involved deciding between a fixed pitch amplitude or baseline controls, the usage of wake steering not decrease as $\phi_{max\ abs}$ increases (see Fig. 13). Further, yaw offsets

https://doi.org/10.5194/wes-2025-250
Preprint. Discussion started: 28 November 2025


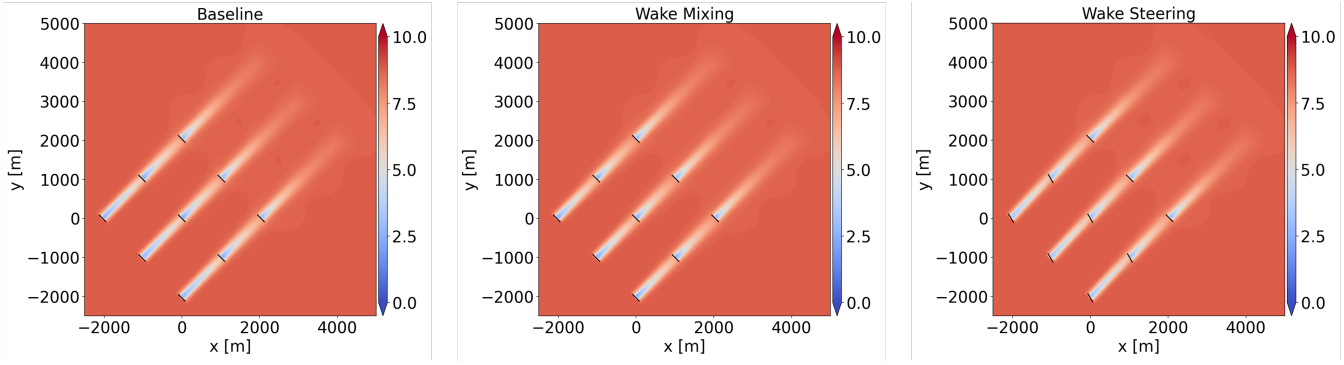


**Figure 16.** An example steady-state flow field from FLORIS simulations of a baseline case (left), an $A = 4°$ wake mixing case (center), and a $\phi_{max\ abs} = 15°$ wake steering case (right). The wind farm is orientated at $225°$ and the turbines are spaced $6D$ apart. The wind condition corresponds to that of the LES considered in Sec. 2, with a wind speed of $9$ m/s, a wind direction of $225°$, and a TI of $3.1\%$.

are permitted on downstream turbines during the Serial-Refine optimization, which is consistent with the AWM optimizer that allowed for mid-farm actuation. Similarly, wake steering is permitted only for wind speeds below $15$ m/s and TI levels below $10\%$, aligning with the AWM optimization process and corresponding to conditions where previous studies have identified the greatest benefits of wake steering (Simley et al., 2020). The power of a turbine under yaw misalignment is represented using a cosine term with an exponent as determined by the "cosine-loss" operational model in FLORIS (NREL, 2025).

In Fig. 15, the optimized wake steering results for farm power gain are shown as a function of the maximum absolute yaw angle, $\phi_{max;abs}$, and for turbine spacings range from $3D$ to $8D$. The results are shown for the same five sets of wind conditions that were considered in Fig. 12. For the first wind condition that was considered in the LES study, wake steering leads to power increases that range from $1\%$ to $7\%$ as the maximum yaw angle increases from $5°$ to $25°$ and the turbine spacing decreases from $8D$ to $3D$. A comparison of streamwise velocity on the hub-height plane between a baseline case, a wake mixing case, and a wake steering case in this wind condition is shown in Fig. 16. For the partially-waked wind conditions where the wind direction is restricted to $225° \pm 0.5°$, wake steering increases power generation from $0.25\%$ up to $5\%$ for wind speeds less than $15$ m/s and TI levels less than $10\%$, and up to $2.5\%$ when all wind speeds and TI levels are considered. Finally, for the fifth set of wind conditions that includes the entire Weibull distribution, wake steering results in AEP gains ranging from $0.1\%$ and $1.2\%$ over baseline operations, with AEP gains over $1\%$ only occurring for the smallest turbine spacing and largest values of $\phi_{max\ abs}$. Note that these large values of $\phi_{max\ abs}$ may be achievable in practice; for example, Damiani et al. (2018) examined loads implications of yaw offset angles up to $25°$ for a 5MW turbine.

As with wake mixing, these gains in farm power can be contextualized by how often wake steering is used across the Weibull distribution, as was shown in Fig. 13. Wake steering is used to maximize farm power for between $13\%$ and $32\%$ of wind conditions as the turbine spacing increases from $3D$ to $8D$. For the wind conditions where wake steering is used on at least one turbine, the total farm power is increased by roughly $1\%$ to $3\%$ over baseline operations (see Fig. 15), which is similar to the power gains observed when AWM is used.

https://doi.org/10.5194/wes-2025-250
Preprint. Discussion started: 28 November 2025


eawe european academy of wind energy
Open Access WIND ENERGY SCIENCE DISCUSSIONS

## 5 Conclusions

This study addressed three critical needs for evaluating AWM strategies in a wind farm. First, a series of high fidelity LES were performed of a $3 \times 3$ wind farm that included multiple turbine layouts and control parameters. The LES extended the two-turbine results from Frederik et al. (2025a) and Brown et al. (2025) to the case of a larger array of wind turbines. Overall, the results demonstrated the effectiveness of AWM in enhancing power generation, particularly for tightly spaced, geometrically aligned wind farms in stable ABLs. While the conventional pulse method performed the best at enhancing the power generation of second row turbines, the helix method led to a greater improvement for third row turbines, primarily driven by a sustained increase in turbulent entrainment of mean-kinetic energy in the wake of the second-row turbines. A similar trend was observed when forcing the pulse method at a subharmonic frequency of $St = 0.15$ versus $St = 0.3$, although the total farm power for the subharmonic case did not exceed the conventional value. Having been found to demonstrate appropriately good power performance for the 3 x 3 array, the high-fidelity results and specifically those of the pulse cases were leveraged to provide relevant training data for the reduced-order model.

Second, a framework for estimating AEP was developed within the FLORIS toolkit. Building on Frederik et al. (2024), a model for AWM was added to the wake mixing term in the empirical Gaussian model, and a model for the power and thrust of actuated turbines was developed based on LES data. A calibration routine was developed for tuning the FLORIS model parameters to LES data, and an optimization routine was built for determining the optimal use of AWM through the farm for maximizing AEP. AEP estimates were determined using Weibull data gathered from the NY Bight, providing an insight into the potential benefits of AWM in real-world scenarios. Farm power gains as a function of pitch amplitude ranging from $A = 1°$ to $6°$ were provided for turbine spacings $3D$ to $8D$, generally indicated gains of $1\%$ to $3\%$ when AWM was being used (around $10\%$ to $30\%$ of the time), which translated to AEP gains of $0.1\%$ to $0.4\%$.

Third, the farm power gains for wake mixing were compared to wake steering using the yaw-optimization routines in FLORIS and the LES-calibrated baseline empirical Gaussian model. Farm power gains were shown as a function of the maximum absolute yaw offset angle, ranging from $\phi_{max\ abs} = 5°$ to $25°$, and turbine spacing ranging from $3D$ to $8D$. Baseline-normalized power gains of $1\%$ to $3\%$ were also observed when wake steering was being used, which translated to AEP gains of $0.2\%$ to $0.8\%$ for most of the turbine spacings and maximum absolute yaw angles considered. Although the baseline-normalized farm power gains are largely similar between wake mixing and wake steering, the results do generally support the findings of Taschner et al. (2024), who showed that wake steering is preferred to wake mixing except in fully-waked configurations.

The AEP gains for both wake mixing and wake steering indicate that some caution is advised when extrapolating from the type of ideal scenarios typically examined in wind farm flow control studies to the comprehensive range of wind conditions a turbine might encounter during annual operations. When interpreting these results, it is important to remember that FLORIS is a low-fidelity steady-state engineering model, and there are many sources of uncertainty in both the model formulation and the tuning of parameters based on a limited set of training data. Future work aimed at quantifying this uncertainty relative the predicted percentages of AEP gain would greatly enhance the utility of FLORIS for evaluating turbine control strategies.

https://doi.org/10.5194/wes-2025-250
Preprint. Discussion started: 28 November 2025


eawe european academy of wind energy
Open Access WIND ENERGY SCIENCE DISCUSSIONS

Further, the results presented here should be used to inform a wider sweep of higher-fidelity simulations to build confidence in the results, including additional LES cases or more sophisticated reduced order models that capture the unsteady wake dynamics induced by AWM (Cheung et al., 2024a; Muscari et al., 2022; Gutknecht et al., 2023). Lastly, turbine loads should be examined alongside power gains to provide a more comprehensive economic picture of wake mixing control strategies (Frederik and van Wingerden, 2022).

*Code availability.* The code used to perform the LES for this study is available as part of the ExaWind software suite: https://github.com/Exawind. The FLORIS software is available at https://github.com/NREL/floris.

*Data availability.* The datasets generated for this paper are available upon request.

*Author contributions.* Sandia (GRY, KB, LC, ND, DH) conducted the precursor and wind turbine LES, analyzed the LES data, performed the FLORIS simulations, developed the calibration and control optimization routines, analyzed the FLORIS results and prepared the manuscript. GE (BJ) consulted on the LES cases and FLORIS analysis.

*Competing interests.* The contact author has declared that none of the authors has any competing interests.

*Disclaimer.* Any subjective views or opinions that might be expressed in the written work do not necessarily represent the views of the U.S. Government. The U.S. Government retains and the publisher, by accepting the article for publication, acknowledges that the U.S. Government retains a nonexclusive, paid-up, irrevocable, worldwide license to publish or reproduce the published form of this work, or allow others to do so, for U.S. Government purposes. The DOE will provide public access to results of federally sponsored research in accordance with the DOE Public Access Plan. The views expressed in the article do not necessarily represent the views of the U.S. DOE or the U.S. Government.

*Acknowledgements.* The authors would like to express their gratitude to Dr. Joeri Frederik and Dr. Misha Sinner for their help with the FLORIS code development and their insightful feedback on the presentation of this work at NAWEA/WindTech 2025.

Sandia National Laboratories is a multi-mission laboratory managed and operated by National Technology & Engineering Solutions of Sandia, LLC, a wholly owned subsidiary of Honeywell International Inc., for the U.S. Department of Energy's National Nuclear Security Administration under contract DE-NA0003525.

This research used resources of the Oak Ridge Leadership Computing Facility at the Oak Ridge National Laboratory, which is supported by the Office of Science of the U.S. Department of Energy under the National Renewable Energy Laboratory's Contract No. DE-AC05-00OR22725, and under the ALCC allocation "Grand-challenge predictive wind farm simulations".

https://doi.org/10.5194/wes-2025-250
Preprint. Discussion started: 28 November 2025


*Financial support.* This research has been supported in part by the Wind Energy Technologies Office within the Office of Energy Efficiency and Renewable Energy (grant no. 40245) and by the Office of Technology Commercialization under award number 1024025-FY24 TCF-23SN020126.

https://doi.org/10.5194/wes-2025-250
Preprint. Discussion started: 28 November 2025


eawe european academy of wind energy
Open Access WIND ENERGY SCIENCE DISCUSSIONS

## References

Almgren, A. S., Bell, J. B., Colella, P., Howell, L. H., and Welcome, M. L.: A conservative adaptive projection method for the variable density incompressible Navier–Stokes equations, Journal of Computational Physics, 142, 1–46, 1998.

Brown, K., Houck, D., Maniaci, D., Westergaard, C., and Kelley, C.: Accelerated Wind-Turbine Wake Recovery Through Actuation of the Tip-Vortex Instability, AIAA Journal, 60, 3298–3310, 2022.

Brown, K., Bortolotti, P., Branlard, E., Chetan, M., Dana, S., deVelder, N., Doubrawa, P., Hamilton, N., Ivanov, H., Jonkman, J., et al.: One-to-one aeroservoelastic validation of operational loads and performance of a 2.8 MW wind turbine model in OpenFAST, Wind Energy Science, 9, 1791–1810, 2024.

Brown, K., Yalla, G., Cheung, L., Frederik, J., deVelder, N., Houck, D., Simley, E., and Fleming, P.: Comparison of wind farm control strategies under a range of realistic wind conditions: wake quantities of interest, Wind Energy Science, 2025.

Cheung, L., Yalla, G., Mohan, P., Hsieh, A., Brown, K., deVelder, N., Houck, D., and Henry de Frahan, M.: Modeling the effects of active wake mixing on wake behavior through large scale coherent structures, Wind Energy Science, 2024, 1–26, 2024a.

Cheung, L. C., Brown, K. A., Houck, D. R., and Develder, N. B.: Fluid-dynamic mechanisms underlying wind turbine wake control with Strouhal-timed actuation, Energies, 17, 865, 2024b.

Commission, I. E.: 12-1: Power Performance Measurements of Electricity Producing Wind Turbines, British Standard, IEC, 2017.

Damiani, R., Dana, S., Annoni, J., Fleming, P., Roadman, J., van Dam, J., and Dykes, K.: Assessment of wind turbine component loads under yaw-offset conditions, Wind Energy Science, 3, 173–189, 2018.

Doekemeijer, B. M., van der Hoek, D., and van Wingerden, J.-W.: Closed-loop model-based wind farm control using FLORIS under time-varying inflow conditions, Renewable Energy, 156, 719–730, 2020.

Fleming, P. A., Stanley, A. P., Bay, C. J., King, J., Simley, E., Doekemeijer, B. M., and Mudafort, R.: Serial-refine method for fast wake-steering yaw optimization, in: Journal of Physics: Conference Series, vol. 2265, p. 032109, IOP Publishing, 2022.

Frederik, J., Doekemeijer, B., Mulders, S., and van Wingerden, J.-W.: On wind farm wake mixing strategies using dynamic individual pitch control, in: Journal of Physics: Conference Series, vol. 1618, p. 022050, IOP Publishing, 2020a.

Frederik, J., Sinner, M., and Fleming, P.: An engineering approach to modeling active wake mixing, 2024.

Frederik, J., Simley, E., Brown, K., Yalla, G., Cheung, L., and Fleming, P.: Comparison of wind farm control strategies under a range of realistic wind conditions: turbine quantities of interest, Wind Energy Science, 2025a.

Frederik, J. A. and van Wingerden, J.-W.: On the load impact of dynamic wind farm wake mixing strategies, Renewable Energy, 194, 582–595, 2022.

Frederik, J. A., Doekemeijer, B. M., Mulders, S. P., and van Wingerden, J.-W.: The helix approach: Using dynamic individual pitch control to enhance wake mixing in wind farms, Wind Energy, 23, 1739–1751, 2020b.

Frederik, J. A., Weber, R., Cacciola, S., Campagnolo, F., Croce, A., Bottasso, C., and van Wingerden, J.-W.: Periodic dynamic induction control of wind farms: proving the potential in simulations and wind tunnel experiments, Wind Energy Science, 5, 245–257, 2020c.

Frederik, J. A., Simley, E., Brown, K. A., Yalla, G. R., Cheung, L. C., and Fleming, P. A.: Comparison of wind farm control strategies under realistic offshore wind conditions: turbine quantities of interest, Wind Energy Science, 10, 755–777, 2025b.

Gaertner, E., Rinker, J., Sethuraman, L., Zahle, F., Anderson, B., Barter, G. E., Abbas, N. J., Meng, F., Bortolotti, P., Skrzypinski, W., et al.: IEA wind TCP task 37: definition of the IEA 15-megawatt offshore reference wind turbine, Tech. rep., National Renewable Energy Lab.(NREL), Golden, CO (United States), 2020.

https://doi.org/10.5194/wes-2025-250
Preprint. Discussion started: 28 November 2025


Gutknecht, J., Becker, M., Muscari, C., Lutz, T., and van Wingerden, J.-W.: Scaling DMD modes for modeling Dynamic Induction Control wakes in various wind speeds, in: 2023 IEEE Conference on Control Technology and Applications (CCTA), pp. 574–580, IEEE, 2023.

Gutknecht, J., Becker, M., Taschner, E., Stipa, S., Allaerts, D., Viré, A., and Van Wingerden, J.-W.: Active Cluster Wake Mixing, in: Journal of Physics: Conference Series, vol. 2767, p. 092052, IOP Publishing, 2024.

Hsieh, A., Cheung, L., Blaylock, M., Brown, K., Houck, D., Herges, T., deVelder, N., Maniaci, D., Yalla, G., Sakievich, P., Radunz, W., and Carmo, B.: Model Intercomparison of the ABL, Turbines, and Wakes Within the AWAKEN Wind Farms under Neutral Stability Conditions, Journal of Renewable and Sustainable Energy, in review., 2024.

Hsieh, A. S., Cheung, L. C., Blaylock, M. L., Brown, K. A., Houck, D. R., Herges, T. G., Develder, N. B., Maniaci, D. C., Yalla, G. R., Sakievich, P. J., et al.: Model intercomparison of the ABL, turbines, and wakes within the AWAKEN wind farms under neutral stability conditions, Journal of Renewable and Sustainable Energy, 17, 2025.

Iungo, G. V., Viola, F., Camarri, S., Porté-Agel, F., and Gallaire, F.: Linear stability analysis of wind turbine wakes performed on wind tunnel measurements, Journal of Fluid Mechanics, 737, 499–526, 2013.

Kasper, J. H.: Large-scale Interactions between Wind Farms and the Atmosphere, 2025.

Korb, H., Asmuth, H., and Ivanell, S.: The characteristics of helically deflected wind turbine wakes, Journal of Fluid Mechanics, 965, A2, 2023.

Li, Z. and Yang, X.: Resolvent-based motion-to-wake modelling of wind turbine wakes under dynamic rotor motion, Journal of Fluid Mechanics, 980, A48, 2024.

Li, Z., Li, Y., and Yang, X.: Large eddy simulation and linear stability analysis of active sway control for wind turbine array wake, Physics of Fluids, 36, 2024.

Lignarolo, L., Ragni, D., Scarano, F., Ferreira, C. S., and Van Bussel, G.: Tip-vortex instability and turbulent mixing in wind-turbine wakes, Journal of Fluid Mechanics, 781, 467–493, 2015.

Marten, D., Paschereit, C. O., Huang, X., Meinke, M., Schroeder, W., Mueller, J., and Oberleithner, K.: Predicting wind turbine wake breakdown using a free vortex wake code, AIAA Journal, 58, 4672–4685, 2020.

Mason, J.: Energy Assessment Report, Tech. Rep. 10124962, DNV, 2022.

Medici, D. and Alfredsson, P. H.: Measurements on a wind turbine wake: 3D effects and bluff body vortex shedding, Wind Energy, 9, 219–236, https://doi.org/https://doi.org/10.1002/we.156, 2006.

Meyers, J., Bottasso, C., Dykes, K., Fleming, P., Gebraad, P., Giebel, G., Göçmen, T., and van Wingerden, J.-W.: Wind farm flow control: prospects and challenges, Wind Energy Science, 7, 2271–2306, https://doi.org/10.5194/wes-7-2271-2022, 2022.

Munters, W. and Meyers, J.: Towards practical dynamic induction control of wind farms: analysis of optimally controlled wind-farm boundary layers and sinusoidal induction control of first-row turbines, Wind Energy Science, 3, 409–425, 2018.

Muscari, C., Schito, P., Viré, A., Zasso, A., Van Der Hoek, D., and Van Wingerden, J.: Physics informed DMD for periodic dynamic induction control of wind farms, in: Journal of Physics: Conference Series, vol. 2265, p. 022057, IOP Publishing, 2022.

National Renewable Energy Laboratory: ROSCO v2.8.0, https://github.com/NREL/ROSCO, 2024a.

National Renewable Energy Laboratory: OpenFAST, https://github.com/OpenFAST/openfast, 2024b.

NREL: FLORIS, Version 4.4, https://github.com/nrel/floris, 2025.

Okulov, V. L., Naumov, I. V., Mikkelsen, R. F., Kabardin, I. K., and Sørensen, J. N.: A regular Strouhal number for large-scale instability in the far wake of a rotor, Journal of Fluid Mechanics, 747, 369–380, 2014.

https://doi.org/10.5194/wes-2025-250
Preprint. Discussion started: 28 November 2025


Sarmast, S., Dadfar, R., Mikkelsen, R. F., Schlatter, P., Ivanell, S., Sørensen, J. N., and Henningson, D. S.: Mutual inductance instability of the tip vortices behind a wind turbine, Journal of Fluid Mechanics, 755, 705–731, 2014.

Sharma, A., Brazell, M. J., Vijayakumar, G., Ananthan, S., Cheung, L., deVelder, N., Henry de Frahan, M. T., Matula, N., Mullowney, P., Rood, J., Sakievich, P., Almgren, A., Crozier, P. S., and Sprague, M.: ExaWind: Open-source CFD for hybrid-RANS/LES geometry-resolved wind turbine simulations in atmospheric flows, Wind Energy, 27, 225–257, https://doi.org/https://doi.org/10.1002/we.2886, 2024.

Shid-Moosavi, S., Di Cioccio, F., Tronci, E. M., Haghi, R., Moaveni, B., Liberatore, S., and Hines, E.: Modeling and Experimentally-Driven Sensitivity Analysis of Wake-Induced Power Loss in Offshore Wind Farms: Insights from Block Island Wind Farm, Available at SSRN 4972515, 2024.

Simley, E., Fleming, P., and King, J.: Design and analysis of a wake steering controller with wind direction variability, Wind Energy Science, 5, 451–468, 2020.

Sørensen, J. N.: Instability of helical tip vortices in rotor wakes, Journal of Fluid Mechanics, 682, 1–4, 2011.

Sorensen, J. N. and Shen, W. Z.: Numerical modeling of wind turbine wakes, J. Fluids Eng., 124, 393–399, 2002.

Sprague, M., Ananthan, S., Vijayakumar, G., and Robinson, M.: ExaWind: A multi-fidelity modeling and simulation environment for wind energy, in: J. Phys. Conf. Series, 2020.

Sverdrup, K., Nikiforakis, N., and Almgren, A.: Highly parallelisable simulations of time-dependent viscoplastic fluid flow with structured adaptive mesh refinement, Physics of Fluids, 30, 2018.

Taschner, E., van Vondelen, A. A., Verzijlbergh, R., and van Wingerden, J.-W.: On the performance of the helix wind farm control approach in the conventionally neutral atmospheric boundary layer, in: Journal of Physics: Conference Series, vol. 2505, p. 012006, IOP Publishing, 2023.

Taschner, E., Becker, M., Verzijlbergh, R., and Van Wingerden, J.: Comparison of helix and wake steering control for varying turbine spacing and wind direction, in: Journal of Physics: Conference Series, vol. 2767, p. 032023, IOP Publishing, 2024.

Thomas, J. J., Baker, N. F., Malisani, P., Quaeghebeur, E., Sanchez Perez-Moreno, S., Jasa, J., Bay, C., Tilli, F., Bieniek, D., Robinson, N., et al.: A comparison of eight optimization methods applied to a wind farm layout optimization problem, Wind Energy Science, 8, 865–891, 2023.

Van Beek, M. T., Viré, A., and Andersen, S. J.: Sensitivity and uncertainty of the floris model applied on the lillgrund wind farm, Energies, 14, 1293, 2021.

van Binsbergen, D., Daems, P.-J., Verstraeten, T., Nejad, A. R., and Helsen, J.: Hyperparameter tuning framework for calibrating analytical wake models using SCADA data of an offshore wind farm, Wind Energy Science, 9, 1507–1526, 2024.

van Vondelen, A. A., Coquelet, M., Navalkar, S. T., and van Wingerden, J.-W.: Synchronized Helix wake mixing control, Wind Energy Science, 10, 2411–2433, 2025.

Yalla, G.: Actuator Line Model Calibration, https://exawind.github.io/amr-wind/walkthrough/calibration.html, accessed: 2024-10-30, 2024.

Yalla, G. R., Brown, K., Cheung, L., Houck, D., deVelder, N., and Hamilton, N.: Spectral proper orthogonal decomposition of active wake mixing dynamics in a stable atmospheric boundary layer, Wind Energy Science Discussions, 2025, 1–36, 2025.

Yılmaz, A. E. and Meyers, J.: Optimal dynamic induction control of a pair of inline wind turbines, Physics of Fluids, 30, 085 106, 2018.